UCRL 2953

UNCLASSIFIED

UNIVERSITY OF CALIFORNIA

Radiation Laboratory

π^+-PHOTOMESON PRODUCTION FROM HYDROGEN, DEUTERIUM, HELIUM, AND CARBON

TWO-WEEK LOAN COPY

This is a Library Circulating Copy which may be borrowed for two weeks. For a personal retention copy, call Tech. Info. Division, Ext. 5545

DISCLAIMER

This document was prepared as an account of work sponsored by the United States Government. While this document is believed to contain correct information, neither the United States Government nor any agency thereof, nor the Regents of the University of California, nor any of their employees, makes any warranty, express or implied, or assumes any legal responsibility for the accuracy, completeness, or usefulness of any information, apparatus, product, or process disclosed, or represents that its use would not infringe privately owned rights. Reference herein to any specific commercial product, process, or service by its trade name, trademark, manufacturer, or otherwise, does not necessarily constitute or imply its endorsement, recommendation, or favoring by the United States Government or any agency thereof, or the Regents of the University of California. The views and opinions of authors expressed herein do not necessarily state or reflect those of the United States Government or any agency thereof or the Regents of the University of California.

UCRL-2953
Unclassified Physics

UNIVERSITY OF CALIFORNIA

Radiation Laboratory
Berkeley, California

Contract No. W-7405-eng-48

π^+-PHOTOMESON PRODUCTION FROM HYDROGEN, DEUTERIUM, HELIUM, AND CARBON

Gordon W. Repp

(Thesis)

April 12, 1955

Printed for the U. S. Atomic Energy Commission

π^+-PHOTOMESON PRODUCTION

Contents

Abstract 4

I Introduction 5

II Experimental Apparatus and Procedure 6

A. General Description of the Experiment 6

1. 180° Arrangement. 6

2. 143° Arrangement. 8

B. Experimental Details

1. Targets 8

a. Gas 8
b. Solid. 12
c. Liquid 12

2. Collimators 12

3. Channels 15

a. 180° Channel 15
b. 143° Channel 15

4. Absorbers 15

5. Detectors 15

a. Scintillation Counters

(1) Scintillators. 15
(2) Electronics 17

b. Nuclear Emulsions 22

6. Beam Monitor 22

C. Procedure

1. At 180° 22

2. At 143° 24

III Analysis of Data

A. Raw Data and Accidental Background

1. Counters 24

2. Emulsions 31

B. Corrections 32

1. Decay in Flight. 32

2. Nuclear Interaction 35

3. Multiple Scattering in Absorbers 36
4. Other Corrections 37
C. Calculation of Energies 37
D. Calculation of Cross Sections 38
1. Second Differential Cross Section 38
a. From 180° Data 40
(1) Emulsions 40
(2) Counters 41
b. From 143° Data 42
2. First Differential Cross Section 43

IV Results
A. 180° Position
1. $\frac{d^2\sigma}{dEd\Omega}$ for Hydrogen, Deuterium, Helium, Carbon . . 44
2. Deuterium-Hydrogen, Helium-Hydrogen, Carbon-Hydrogen Ratios 44
3. $\frac{d\sigma}{d\Omega}$ for Hydrogen 44
B. 143° Position
1. $\frac{d^2\sigma}{dEd\Omega}$ for Hydrogen, Deuterium 53
2. Deuterium-Hydrogen Ratio 53
3. π^-/π^+ Ratio from Deuterium 53
4. $\frac{d\sigma}{d\Omega}$ for Hydrogen 59

V Discussion 59

Acknowledgments 70

References 71

π^+-PHOTOMESON PRODUCTION FROM HYDROGEN, DEUTERIUM, HELIUM, AND CARBON

Gordon W. Repp

Radiation Laboratory
University of California
Berkeley, California

April 12, 1955

ABSTRACT

Hydrogen, deuterium, helium, and carbon were bombarded by the 342 ± 6-Mev bremsstrahlung beam of the Berkeley synchrotron and π^+-mesons were observed at $180^\circ \pm 3^\circ$ to the beam; π^+-mesons were also observed from hydrogen and deuterium at $143^\circ \pm 6^\circ$. At 180° the mesons were deflected out of the photon beam by means of a magnet.

Detection was accomplished by stopping the π^+-meson in a scintillator and detecting the positron from the μ^+-meson decay by a coincidence with a gate triggered by the stopping π^+. Absolute cross sections were obtained by calibrating the scintillation counters with nuclear emulsions. The emulsions were exposed to mesons from hydrogen at 180° and from deuterium at 143°. The π^-/π^+ ratios were acquired from the 143° emulsion data.

Energy distributions were obtained for π^+-mesons from the targets at the angles described above. Excitation functions for π^+-mesons from hydrogen at 180° and 143° are given for photon energies of 196 to 325 Mev. Deuterium-hydrogen ratios are given at 180° and 143°, and helium-hydrogen and carbon-hydrogen ratios are given at 180°.

The hydrogen results are compared to a theory of Chew. The deuterium-hydrogen ratios are compared to a phenomenological calculation by Chew and Lewis.

π^+-PHOTOMESON PRODUCTION FROM HYDROGEN, DEUTERIUM, HELIUM, AND CARBON

Gordon W. Repp

Radiation Laboratory
University of California
Berkeley, California

April 12, 1955

I. INTRODUCTION

Since 1949, when McMillan and Peterson[1] first produced photomesons artificially, a number of photomeson experiments have been performed.[2-37] Of particular interest is the photoproduction of mesons in hydrogen and deuterium,[13-30] because these processes provide a test for meson theories of nuclear forces in their simplest form.

This experiment was designed primarily to contribute to the completion of the experimental picture of photoproduction from hydrogen and deuterium. Toward this end, data were obtained for π^+-mesons at $180^\circ \pm 3^\circ$ and $143^\circ \pm 6^\circ$ to the photon beam. Photoproduction was also obtained at $180^\circ \pm 3^\circ$ to the photon beam for helium and carbon.

The method used in this experiment was to produce mesons in a target and to detect the mesons stopping in a nuclear emulsion or a scintillator placed at the given angle to the beam. For the scintillators the π^+-meson–positron decay was used to detect the mesons. This method was similar to that used by Steinberger and Bishop.[13]

The experimental procedure is described in the next section, the analysis of data is described in Section III, and the results are given in Section IV. The results are discussed and compared with theory in Section V.

II. EXPERIMENTAL APPARATUS AND PROCEDURE

The 180° and the 143° experimental methods were basically the same, but there were differences in the targets, the channels, the scintillators, and the electronics. Therefore, the experiments at the two angles are described concurrently, with subsections as needed.

The arrangement at 180° was designed for use at that angle only; the 143° arrangement was designed for use at all angles between 15° and 165°. The 143° channel and detectors were mounted on a cart which pivoted about the target so that the angle could be easily changed with only a slight modification of the shielding. Data at other angles were not obtained because the low intensity of the synchrotron beam made continuation of the work impractical at the time of the 143° run. If increased beam is obtained in the future, it is hoped that the work can be extended to other angles.

A. General Description of the Experiment

The 342 ± 6-Mev spread-out bremsstrahlung beam of the Berkeley synchrotron was used. This maximum energy is higher than the 322 ± 6 Mev usually quoted in the past.[38] Recent work of Anderson, Kenney, and McDonald[39] gives this higher value, which is confirmed qualitatively by this experiment (Sec. IV, A, 3). The beam was spread out so that each beam pulse was about 4 milleseconds in duration.

1. 180° Arrangement

The beam passed through collimators (Fig. 1) and penetrated a 0.001-inch BeCu window into a vacuum pipe. The vacuum pipe extended through the field of the bending magnet. The target was located within the pipe on the far side of the magnet from the synchrotron. After passing through the target, the beam left the vacuum pipe and then entered a thick-walled ionization chamber. Originally, a clearing magnet was located immediately behind the beam-entrance window of the vacuum pipe; however, it was found that the bending magnet provided sufficient clearing of the electrons. The vacuum was necessary because electrons produced in the air completely masked the meson counts when little or no absorber was used. The mesons that left the target at $180^{\circ} \pm 3^{\circ}$ to the

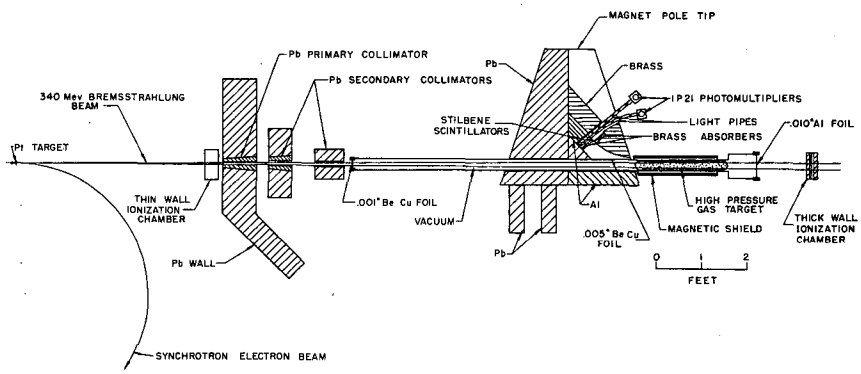

EXPERIMENTAL ARRANGEMENT AT 180°

MUL-586

Fig. 1. Experimental arrangement at 180°.

beam with the proper energy to stop in the detector were bent by the magnetic field down the channel into the detector. In this process the mesons left the vacuum pipe by means of a 0.005-inch BeCu window.

2. 143° Arrangement

The beam passed through the collimators into a vacuum pipe through a 0.001-inch BeCu window (Fig. 2). The pipe, which extended through a clearing magnet and a lead wall, was attached to the target vacuum jacket. The beam passed through the target and out of the vacuum into a thick-walled ionization chamber. The mesons left the target at $143^{\circ} \pm 6^{\circ}$ to the beam and went down the channel into the detectors. In this process the mesons penetrated a 0.001-inch aluminum heat shield and a 0.0045-inch vacuum window.

B. Experimental Details

1. Targets

Three types of target were used: high-pressure, low-temperature gas target (hydrogen, deuterium, or helium) at 180°; solid targets at 180° (carbon and polyethylene); and liquid target (hydrogen or deuterium) at 143°.

a. High-pressure gas target. Figure 3 shows a cutaway view of the high-pressure target. The target proper is a cylindrical vessel 2 inches in diameter and 24 inches long. It is made of stainless steel with end windows 0.040 inch thick. This is the same target described by White et al.[16] but it has been modified considerably. Around the target vessel is a liquid-nitrogen jacket which is connected to a reservoir. Surrounding this jacket and the reservoir is a vacuum jacket. A long evacuated pipe was attached to this vacuum jacket through which the photon beam passed. The target was operated at 2400 psi gauge pressure and at 77° K. This pressure was obtained with the pumping system shown in Fig. 4. One pump was used for hydrogen and helium. A separate pump was used for deuterium to prevent contamination and to permit recovery and reuse. Mass-spectrograph measurements of the deuterium showed 99.21% deuterium, 0.67% air, and 0.11% water. The deuterium is further purified by the liquid-nitrogen trap.

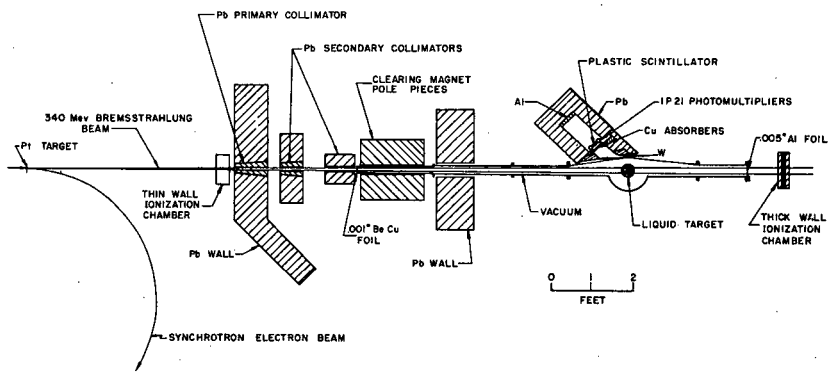

EXPERIMENTAL ARRANGEMENT AT 143°

MUL-585

Fig. 2. Experimental arrangement at 143°.

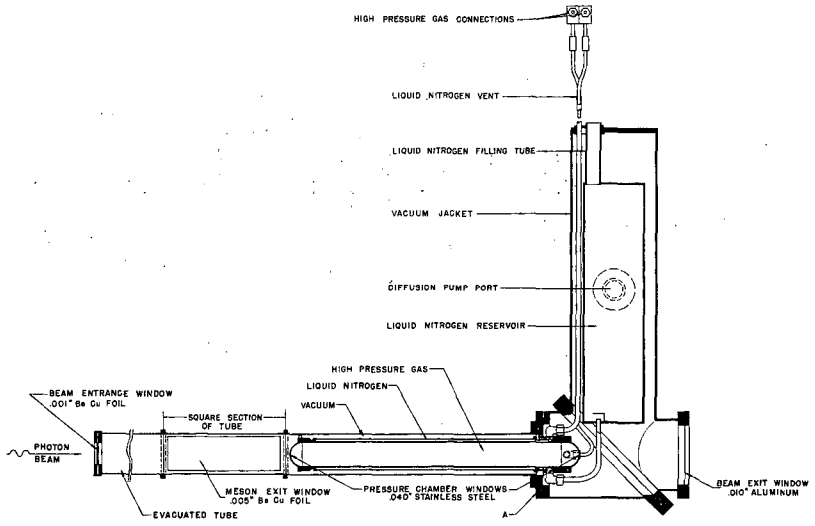

HIGH PRESSURE GAS TARGET

MUL-587

Fig. 3. High-pressure gas target. This target was used at 180° with hydrogen, deuterium, and helium. The target was operated at 2400 psi gauge pressure and 77° K.

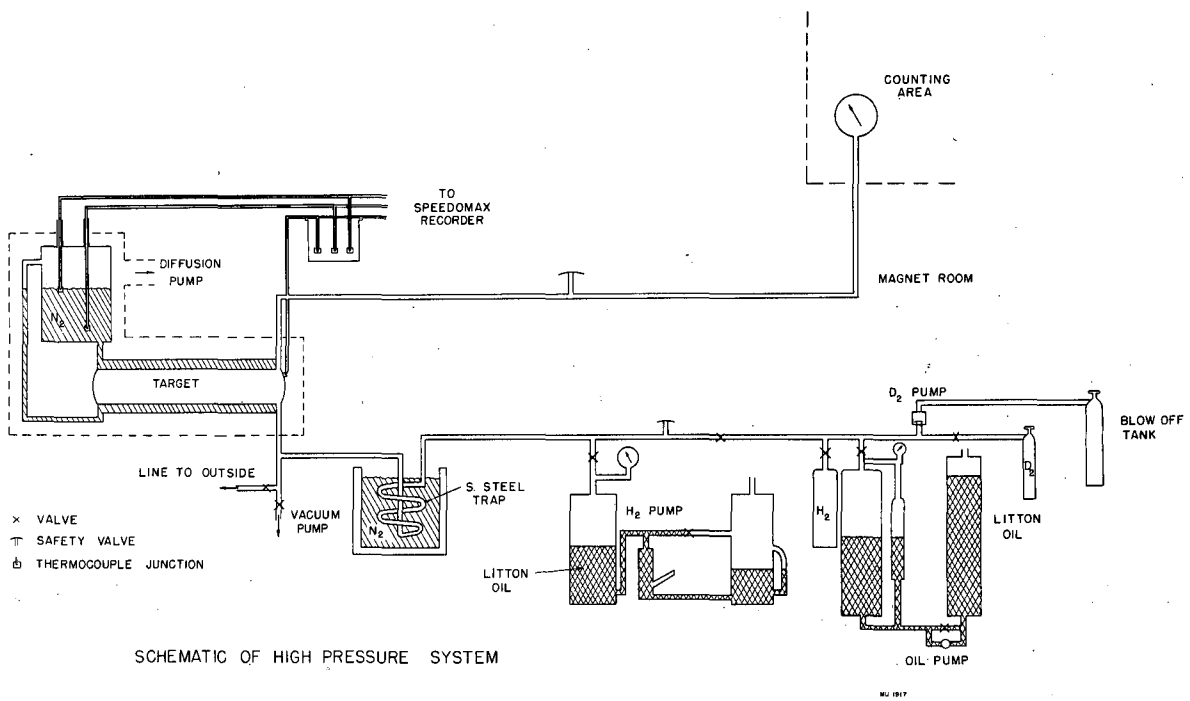

SCHEMATIC OF HIGH PRESSURE SYSTEM

Fig. 4. Schematic drawing of high-pressure pumping system. This system was used with the target in Fig. 3.

b. Solid targets. A carbon disc and a polyethylene disc 2 inches in diameter were used at 180°. Both targets had the same amount of carbon. The gas target was removed from the vacuum pipe by disconnecting it at the flange marked A in Fig. 3. The targets were mounted in styrofoam holders and pushed down the vacuum pipe to the edge of the magnet pole tips. A thin window was then attached to the flange and the tube was evacuated.

c. Liquid target. In Fig. 5 is a cutaway view of the liquid-deuterium target. The target vessel is a cylinder 3 inches in diameter with vertical axis and with 0.003-inch BeCu walls. The heat exchanger was located above the target. It consists of (from the center out) the hydrogen reservoir, the heat-exchanger coils (in vacuum), the liquid-nitrogen reservoir, and the vacuum jacket. The heat-exchanger coil is a helix of two copper tubes soldered together. Liquid hydrogen passes up through one tube of the helix and deuterium gas is fed down through the other.

This latter tube is wound tightly around the liquid hydrogen reservoir before it empties into the liquid-deuterium reservoir. The liquid level in the target is determined by measuring the capacity of capacitors at the top and the bottom of the target. The capacity changes about 4μμf when the dielectric changes from gas to liquid. Figure 6 shows a schematic drawing of the target and the recovery system. Each of the two tanks shown has a capacity of 2,000 liters. Mass-spectrograph measurements of the deuterium showed 96.73% D_2 and 3.27% He in the storage tank and 98.03% D_2 and 1.97% HD at the condenser vent.

For use with hydrogen, the deuterium tanks were disconnected and liquid hydrogen was fed directly into the deuterium tube of the heat exchanger.

2. Collimators

Three lead collimators were used for both arrangements (Figs. 1 and 2). The primary collimator was a lead piece 9.5 inches long. The collimating hole was 0.5 inch in diameter at the side near the synchrotron and increased in diameter toward the far side. The collimator was located 56 inches from the synchrotron target.

The secondary collimators also had inversely tapered holes. They were placed to just clear the beam. All the collimators were carefully aligned with a transit and were checked with x-ray film.

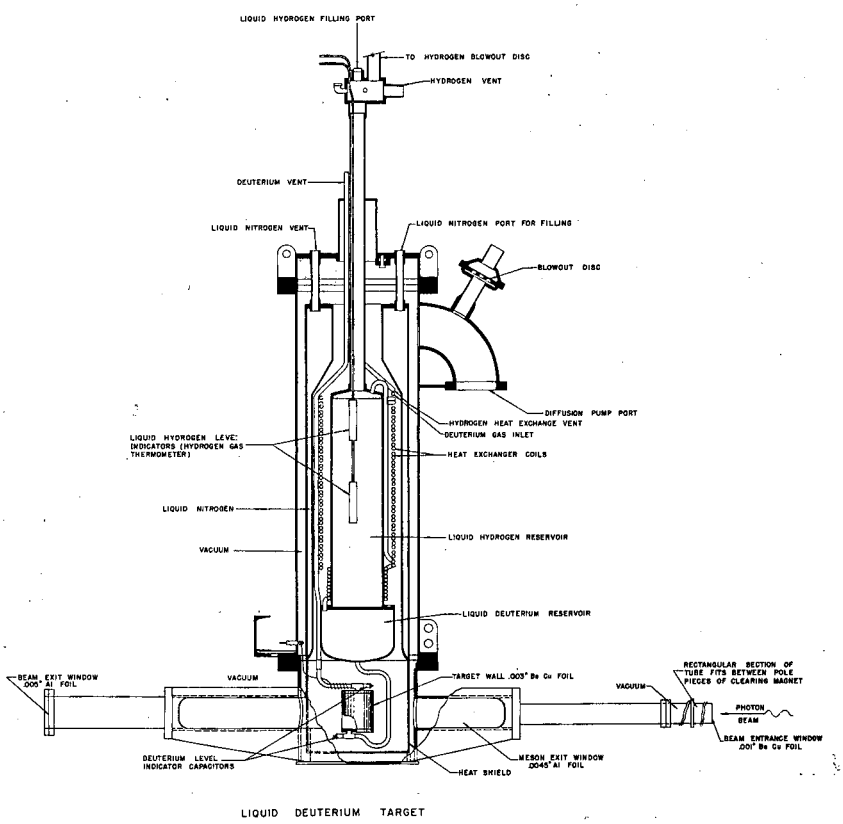

MUL-588

Fig. 5. The liquid-deuterium target. This target was used at 143° with liquid hydrogen and deuterium.

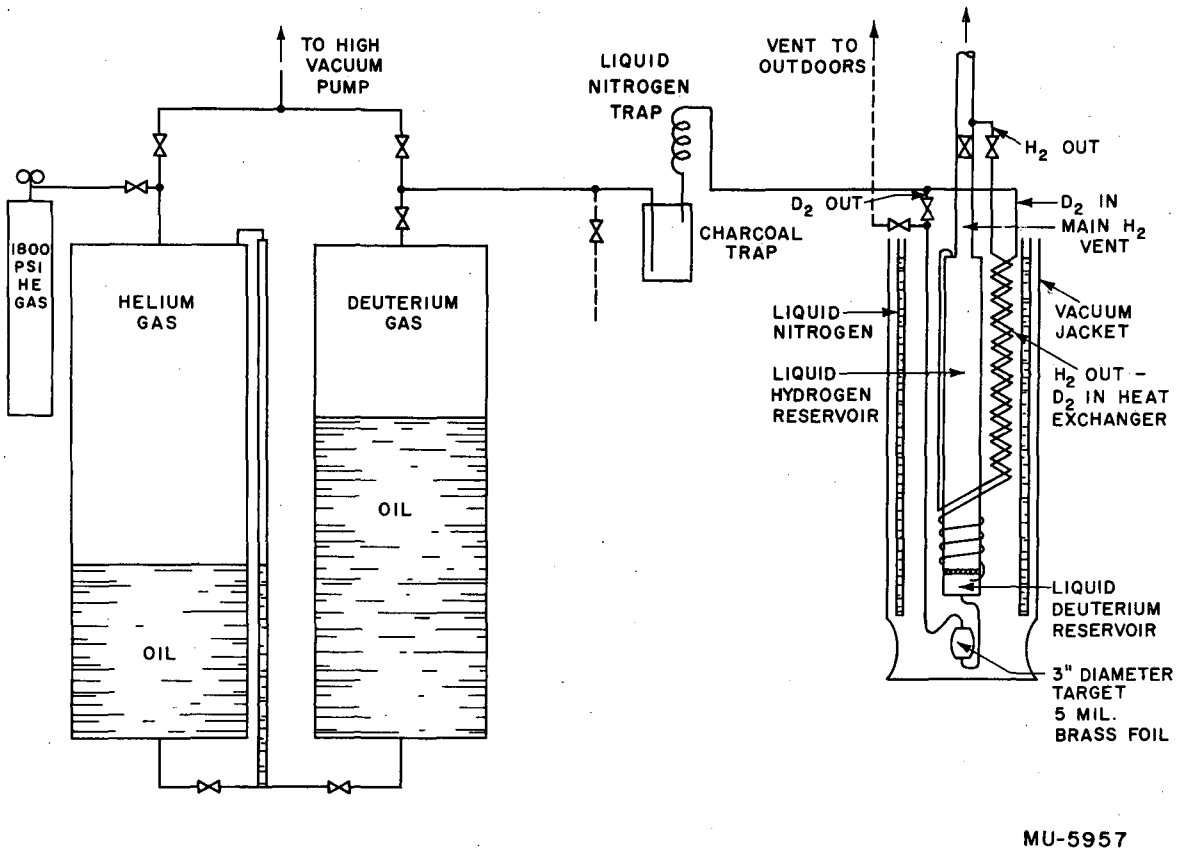

Fig. 6. Schematic drawing of liquid-deuterium target and deuterium-recovery system.

3. Channels

The channel and shielding were designed primarily to cut down electron background.

a. 180° channel. Lead was used on the synchrotron side of the magnet to shield the detectors from high-energy electrons. Aluminum and brass were used on the other side to minimize scattering (Fig. 1). The meson channel had a 14-inch radius, and the field was set at a value to allow mesons of the proper energy to stop in the detector. The energy width of the channel was wide compared to that of the detector. The angular resolution was also determined by the detector and not by the channel. Figure 7 shows the shape of angular resolution. The $\pm 3^{\circ}$ quoted is the width at half intensity.

b. 143° channel. The channel was essentially a lead house around the detector with an opening on one side. (See Fig. 2.) The back of the enclosure was lined with aluminum and was one foot away from the detector. Electron backscattering into the detector was therefore minimized. The angular resolution of the system was determined by the detector and not by the channel. The angular resolution curve was a regular trapezoid with half width of 6° at half intensity and total half width of 11°.

4. Absorbers

The absorbers used with the scintillation counters were placed immediately in front of the scintillators. The absorbers determined the energy of the mesons which stopped in the scintillator and thus determined the energy of the mesons detected. The absorbers were pulled in and out of the channel with wires and they could be varied in 1/32-inch steps from 0 to 1-1/4 inches for 180° or to 1-15/32 inches for 143°. Brass was used as absorber material at 180° while copper was used at 143°.

5. Detectors

Scintillation counters and nuclear emulsions were used to detect the π^{+}-mesons. Scintillators were the primary detection system. Nuclear emulsions were used to determine the absolute efficiency of the counters.

a. Scintillation counters. (1) Scintillators. At 180° two stilbene scintillator crystals were used. The detected mesons passed through the

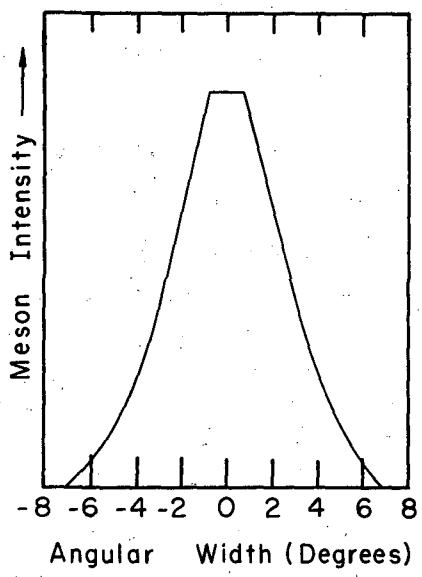

MUL-910

Fig. 7. 180° angular resolution curve.

first and stopped in the second crystal. The first crystal was 3.5 by 3.5 by 3/8 inches, and the second was 2.5 by 2.5 by 0.75 inches. These crystals were mounted on lucite light pipes, each of which was viewed by a 1P21 photomultiplier tube located outside the magnetic field.

At 143° a single plastic scintillator was used. This scintillator was 2 by 2 by 0.75 inches, and it was made of terphenyl in polystyrene. It was viewed directly by two 1P21 photomultiplier tubes. The detected mesons stopped in this scintillator.

(2) Electronics. Figure 8 shows a block diagram of the electronics. The units below the dashed line are the primary detection system, and these units were the same at both angles except for the scintillators and the photomultipliers. Consider the operation at 180° (for this, ignore broken-line connections in Fig. 8). The meson passed through the first scintillator and stopped in the second. Each of the two pulses was fed through attenuators into distributed amplifiers, and each of the two pulses was then sent to multivibrators. The signal from the second scintillator was split after the amplifier and was fed to two multivibrators. Two of the multivibrator outputs -- one from each scintillator -- were fed into a coincidence circuit. The coincidence output triggered four tandem gates each 2 microseconds long. Each of these gates was fed to a coincidence circuit which had the third multivibrator output as the other input. The output of each of these four coincidences was scaled. Thus, a particle which passed through the first scintillator and passed through or stopped in the second scintillator triggered the gates. The first gate was delayed enough so that the signal from the particle passing through the third multivibrator did not form a coincidence with the first gate. If the particle stopped in the second scintillator and decayed during one of the gates, then the signal from the decay particle formed a coincidence and was scaled. The resolution of the electronics was not fast enough to detect the π-μ decay, but could detect the positron of the μ-β decay. Thus, if the particles were π^{+}-mesons, the characteristic decay time of the μ-β decay appeared.

All the electronic circuits were fairly standard. The distributed amplifiers had four stages of amplification. The last of these acted as a limiter by being driven to cutoff by large signals. Thus, the multi-

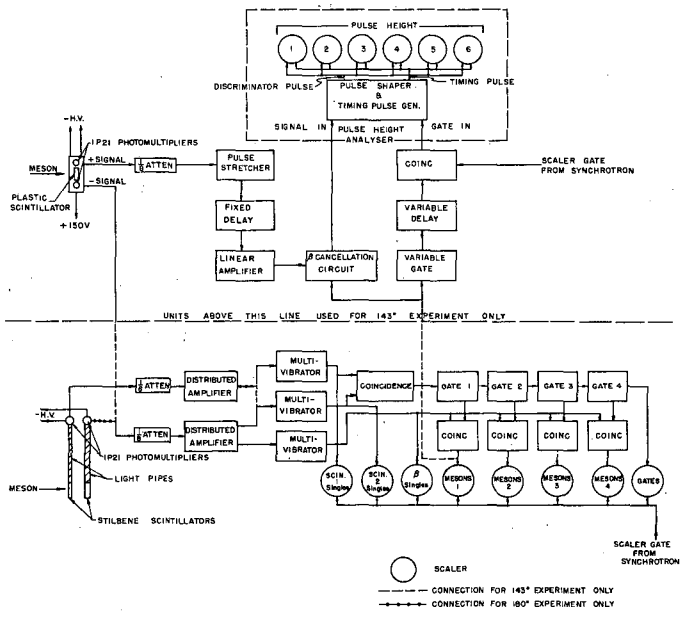

BLOCK DIAGRAM OF ELECTRONICS

MUL-583

Fig. 8. Block diagram of electronics. The primary detection system is below the broken line. The units above the line are for pulse-height analysis of the π pulses.

vibrators were prevented from double pulsing. The multivibrators were of the ringing type (in which a tuned circuit is allowed to ring for a half cycle). The multivibrators provided a uniform pulse regardless of input; by this means the operation of the tandem gate unit was made stable. The coincidence units were of the Rossi type. The tandem gate lengths were determined by delay line, and the trailing edge of each pulse triggered the following gate. The scalers were gated by the synchrotron, thus permitting counting only during the beam pulse.

At 143° the method was identical except that the front scintillator was eliminated. The operation was kept the same, however, by feeding the output from the one scintillator through a distributed amplifier and then splitting the signal and feeding all three multivibrators. (The 143° scintillator is above the dashed line in Fig. 8, and now, broken lines are connections. The lines with dots are to be ignored.) At 143° an attempt was made to measure low-energy mesons. The energy of the stopped mesons was measured by pulse height. No absorber was used. The circuits for this purpose are shown above the dashed line in Fig. 8. This system measured all meson pulses which had decay particles coincident with the first gate of the primary detection system. The output of the first gate coincidence was split, and half was used to trigger the pulse-height analyzer through a standard UCRL variable gate and delay. This signal also triggered the β cancellation circuit, which suppressed the β pulse and allowed only the π pulse to be analyzed. This circuit, designed by William Ganz, is shown in Fig. 9. The signal to be analyzed was taken off the anode of the photomultiplier, whereas the signal to operate the primary detection system came from the last dynode. The signal to be analyzed was fed through a pulse stretcher, a fixed delay, a standard UCRL linear amplifier, and the β-cancellation circuit to the pulse-height analyzer. The pulse-height analyzer consisted of a timing-pulse generator, pulse stretcher, and a standard UCRL scaler for each channel. The pulse-height analyzer is described in a report by Bowman and Thomas.[40] Figure 10 shows the basic operation of the pulse-height analyzer. Channel 1 scales maximum pulse height.

Several precautions were taken to maintain stability in the electronics. All B^{+} supplies and filament power were regulated. All the

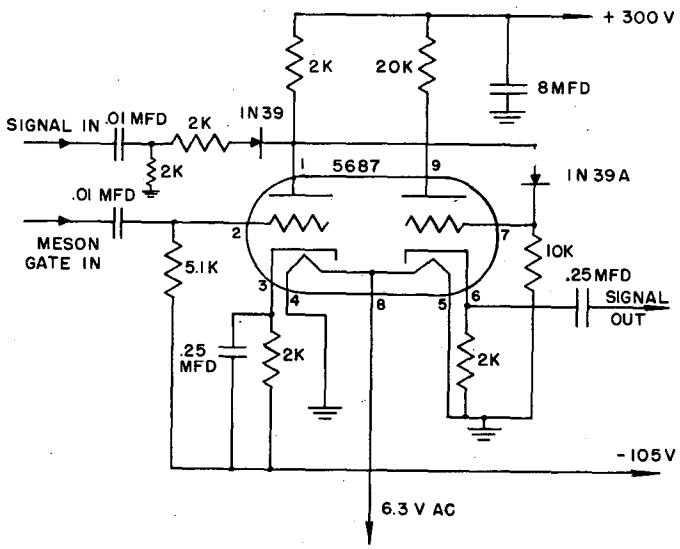

β PULSE CANCELLATION CIRCUIT

MUL-584

Fig. 9. β-pulse cancellation circuit. This circuit suppresses the β pulse, allowing only the π pulse to be pulse-height analyzed.

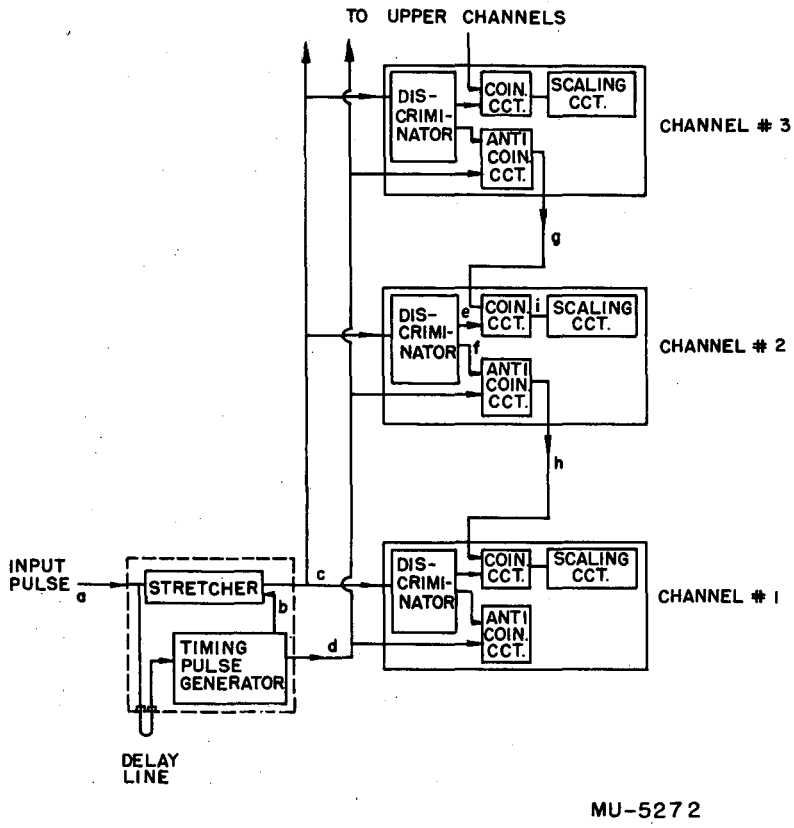

Fig. 10. Block diagram of pulse-height analyzer. Channel 1 is maximum pulse-height channel.

electronics units were kept in a constant-temperature rack. The pulse-height channels were calibrated periodically.

b. Nuclear emulsions. Nuclear emulsions were exposed in the positions that were previously occupied by scintillators in Figs. 1 and 2. The absorbers previously described were removed and were replaced by an aluminum absorber block containing four Ilford C.2 emulsions 1 by 3 inches by 400 microns. The absorber block is shown in Fig. 11. Two emulsions were placed in each slot. The slots were inclined to the meson beam by 8.8°. This arrangement gave an energy distribution of mesons along the emulsion.

6. Beam monitor

The beam was monitored with a thick-walled ionization chamber behind the experiment. (See Figs. 1 and 2.) This chamber was a duplicate of one used at Cornell. The Cornell calibration[41] was checked by the method of Blocker, Kenney, and Panofsky,[42] and agreed within the 10-percent accuracy claimed for this method. A thin-walled chamber was also used in front of the experiment as a check; however, it was not very reliable, as its calibration depended on certain synchrotron operating parameters.

C. Procedure

1. At 180°

The apparatus was set up with the scintillation counters and polyethylene target. Plateaus were run by changing photomultiplier voltages and the output attenuators on the distributed amplifiers. Indication of a plateau was found for the first scintillator and for the π pulses in the second scintillator. The statistics were not very good on these plateaus, and it was decided not to try to improve on them, since emulsions were to be used for calibration. Next the absorbers were changed while the magnetic field was held constant. By this means the magnetic channel was shown to be wide compared to the energy width of the detector.

Each run for data consisted of a certain amount of integrated beam which required about one-half hour. At the end of each run, absorber and magnetic field were changed. Each absorber was run several times throughout the course of the experiment. A standard point was run

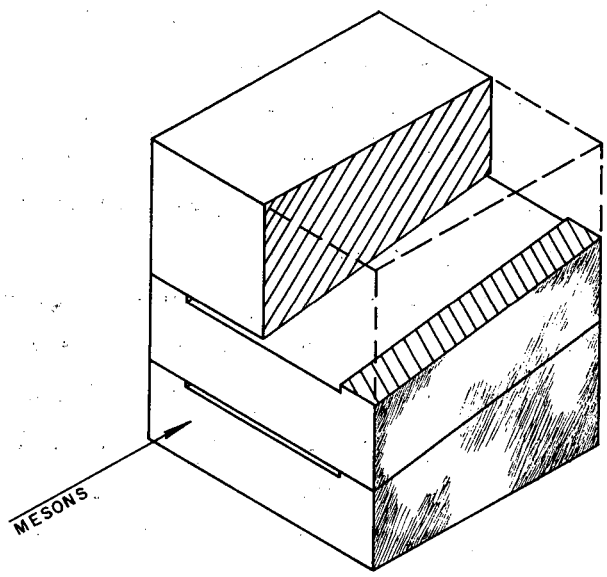

MUL-579

Fig. 11. Emulsion absorber block. Four emulsions were placed in the slots and the block was placed in the meson channel.

several times a day as a check on the efficiency of the detection system. The polyethylene and carbon targets were alternated several times during this part of the experiment.

The gas target was installed and hydrogen, deuterium, helium, and the empty target were run, following the same procedure as above. During this phase of the experiment, π^+-mesons from hydrogen at 47 Mev were used as a check point. The next phase was to expose emulsion to the mesons from hydrogen. The last phase was to check the beam calibration (Sec. II, B, 6). The complete run required three weeks with a running time of 16 hours per day for 5 days per week.

2. At 143°

The procedure followed the same general pattern as for 180° except that the entire run was with the liquid target. The synchrotron beam intensity was quite low during this period. The complete run required 5 weeks at 16 hours per day and 6 days per week plus 3 weeks of 24 hours per day, 6 days per week. During this time there were 32 days when beam intensity was high enough to give usable data. Because of low beam, individual runs were several hours long, which made it impossible to run a check point several times a day. The data, however, appear to be fairly consistent from day to day except for a definite change in the middle of the run when a photomultiplier shorted and had to be replaced. Different efficiencies were established for each part of the run.

At the end of the run the emulsions were exposed to mesons from deuterium and the beam calibration was checked.

IV. ANALYSIS OF DATA

A. Raw Data and Accidental Background

1. Counters

Figures 12 to 17 show the raw data as they were taken, with only the accidental-coincidence background subtracted. The ordinate on these graphs was actually the number of counts per microcoulomb of charge on the thick-walled beam-monitor chamber. The empty-target data also appear on the graphs except for Fig. 15, which shows the solid-target data from both carbon and polyethylene.

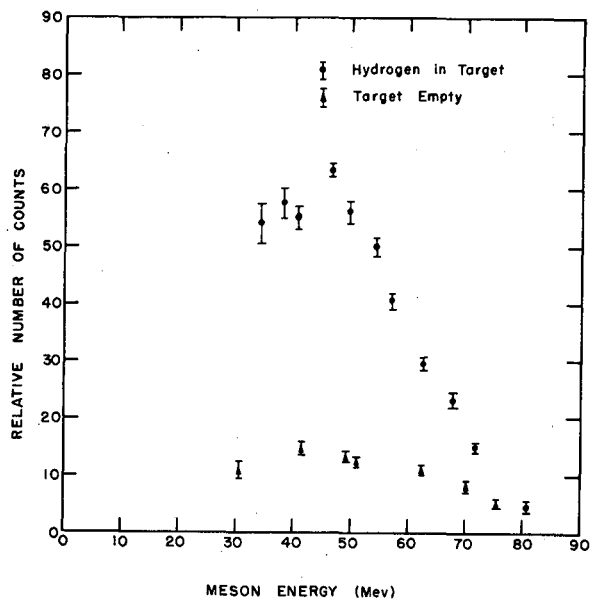

MUL-652

Fig. 12. Raw data for π^+-mesons from hydrogen at 180°. These data have been corrected only for accidental coincidence background. The errors shown are standard deviations. The background from the end walls of the gas target is shown.

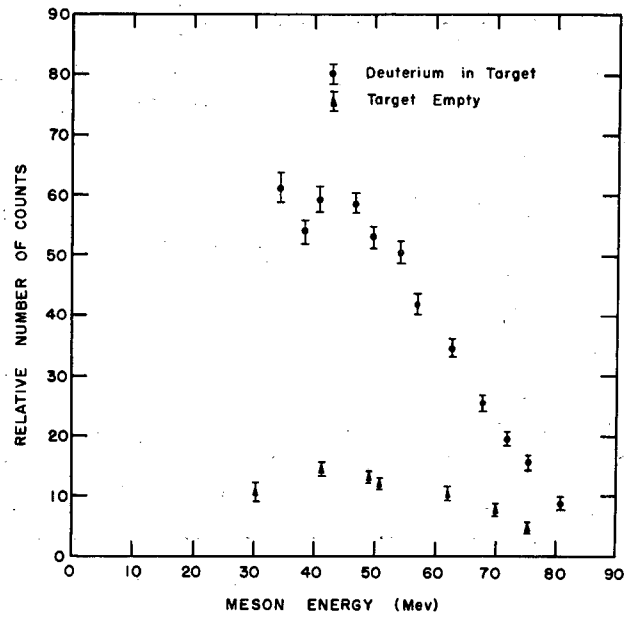

MUL-651

Fig. 13. Raw data from π^+-mesons from deuterium at 180°. These data have been corrected only for accidental coincidence background. The errors shown are standard deviations. The background from the end walls of the gas target is shown.

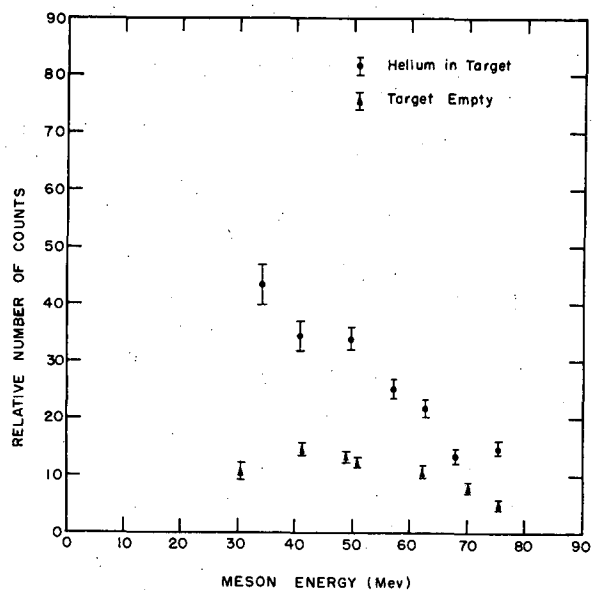

MUL-653

Fig. 14. Raw data for π^+-mesons from helium at 180°. These data have been corrected only for accidental coincidence background. The errors shown are standard deviations. The background from the end walls of the gas target is shown.

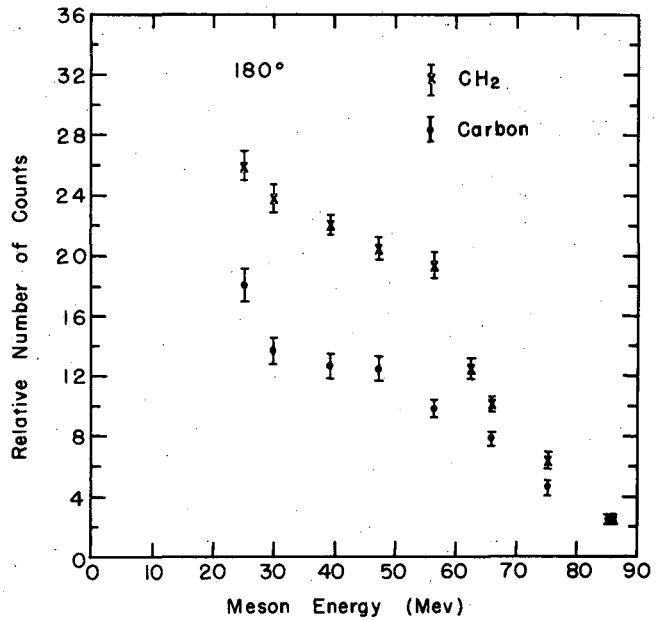

MUL-857

Fig. 15. Raw data for π^+-mesons from polyethylene and carbon at 180°. These data have been corrected only for accidental coincidence background. Both targets had the same amount of carbon. The errors shown are standard deviations.

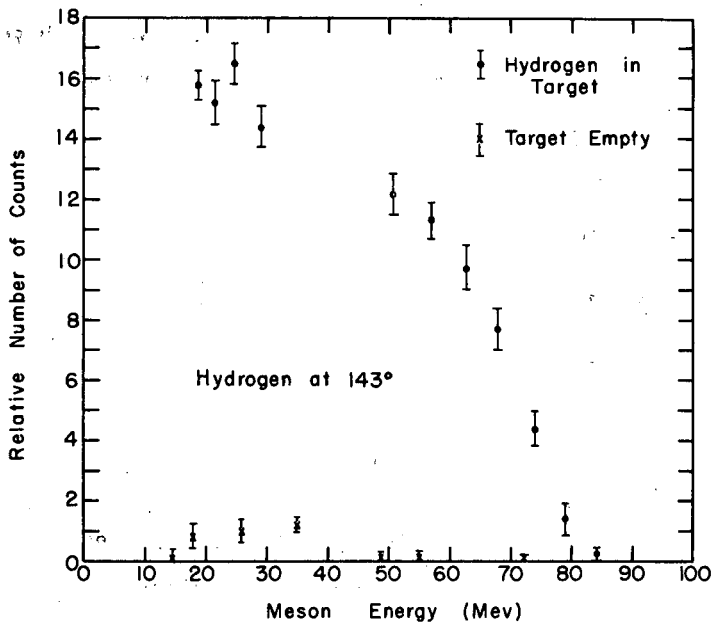

MUL-860

Fig. 16. Raw data for π^+-mesons from hydrogen at 143°. These data have been corrected only for accidental coincidence background. The errors shown are standard deviations. The background from the walls of the liquid target is shown.

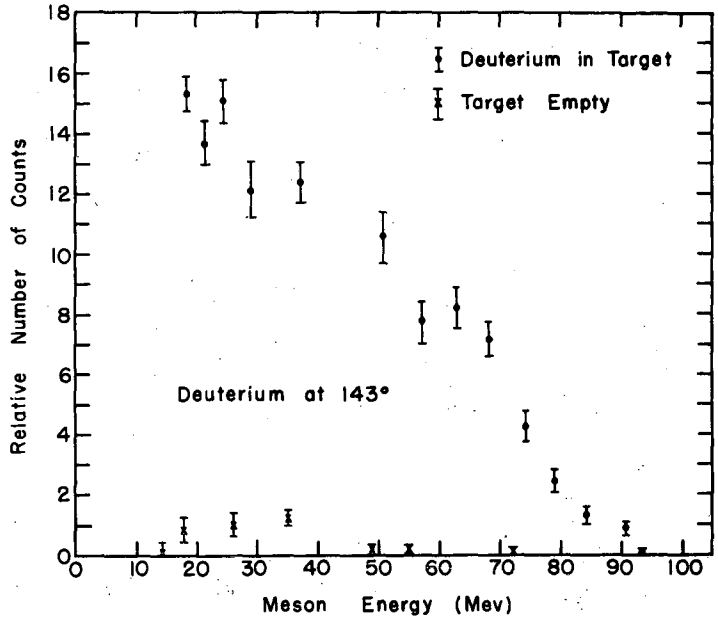

MUL-863

Fig. 17. Raw data for π^+-mesons from deuterium at 143°. These data have been corrected only for accidental coincidence background. The errors shown are standard deviations. The background from the end walls of the liquid target is shown.

The accidental-coincidence background was determined by using the half life of the μ-β decay.[43] When this half life was used, it was possible to calculate the number of mesons that should occur in any gate from the number in any preceding gate. A background due to particles' forming accidental coincidences with the gates appears as a uniform number of particles in each gate superimposed on the decay distribution. The background calculation was accomplished by taking the number of counts in any two gates. The expected number of counts in Gate One was calculated from the actual number of counts in Gate Two. The difference between the actual and the expected counts was identified as the background. Since the background is uniform in both gates, it must be subtracted from the first gate. The subtraction changes the number of counts in the first gate. The new number is then used to calculate a new background by the same process. With successive approximations of the above type, the background quite rapidly converges to a value. This process was carried out with several combinations of gates and an average was taken. The values of background from the various gates agreed quite well with one another, indicating that the proper half life was used and that π^+-mesons were being counted.

2. Emulsions

All emulsion areas were scanned by two observers. The resulting efficiency is estimated to be better than 95%. The mesons were identified by their track endings. Meson endings of the π-μ, ρ, and σ types were observed. The scanning was done with a standard Bausch and Lomb binocular microscope with 53x oil-immersion objectives and 5x eyepieces. Higher power was used for close examination of the endings.

Angular distributions of the mesons were measured, and both the horizontal and the vertical distributions peaked as expected in the target direction. Endings were found to be distributed uniformly with depth in the emulsion except near the surfaces. For this reason, mesons that stopped in the 20 microns of emulsion (before development) next to each surface were discarded. Measurements were made of the emulsion shrinkage during development; a shrinkage factor of 1.975 was found.

At 180° the areas scanned all corresponded to but one energy interval. These emulsions had been exposed to mesons from hydrogen.

At 143° three energy intervals were scanned, and mesons from deuterium were observed. Table I shows the emulsion raw data.

Three σ events are shown at 180° from the hydrogen target. It is possible that π^--mesons formed in the ends of the target can scatter down the channel into the emulsion. Another possibility is that double charge exchange of a π^+ takes place in the absorbers.

Table I

Emulsion raw data

Angle	180°	143°	143°	143°
Meson energy (Mev)	46	13	25	40
Target	hydrogen	deuterium	deuterium	deuterium
Units of integrated photon beam	263	208	208	208
π-μ events	332	50	54	70
σ events	3	43	47	72
Volume scanned (cm^3)	0.2283	0.0764	0.0795	0.1457
π-μ events per cm^3	1454 ± 79	654 ± 93	679 ± 93	482 ± 57
π-μ events per cm^3 unit of integrated beam	5.50 ± 0.30	3.14 ± 0.45	3.26 ± 0.45	2.31 ± 0.27

B. Corrections

Tables II and III show the corrections at 180° and at 143° respectively. The numbers given are the fraction of the total number of mesons, out of those leaving the mean position of the target, that arrive at the detector. The corrections are as follows:

1. Decay in Flight

The fraction of mesons reaching the detector (out of all those that leave the target) is $e^{-\frac{t}{\tau}}$, where: t = the time of flight of the meson in the meson frame and τ = the mean life of the π^+-mesons = 2.54×10^{-8}

Table II

Corrections at 180°

The numbers in the table are the fraction of mesons reaching the detector out of all those that leave the center of the target at mean energy.

Meson Energy for Gas Target (Mev)	Decay in Flight	Multiple Scattering	Nuclear Interaction				Meson Energy for Carbon Target (Mev)
			H	D	He	C	
34	0.874	-----	0.867	0.861	0.871	0.995	25
38	0.886	0.995	0.874	0.867	0.878	0.989	29
42	0.893	0.984	0.875	0.868	0.876	-----	--
47	0.903	0.973	0.877	0.867	0.874	0.974	39
50	0.907	0.984	0.873	0.863	0.871	-----	--
54	0.913	0.972	0.867	0.859	0.864	0.956	47
57	0.916	0.962	0.862	0.854	0.859	-----	--
63	0.921	0.918	0.851	0.842	0.845	0.933	56
68	0.925	0.924	0.837	0.828	0.831	0.916	62
72	0.927	0.920	0.826	0.816	0.819	0.903	66
75	0.929	0.915	0.814	0.804	0.806	-----	--
81	0.932	0.912	0.796	0.786	0.788	0.871	75
--	0.960	0.914	-----	-----	-----	0.830	85

Table III

Corrections at 143°

The numbers in the table are the fraction of mesons reaching the detector out of all those that leave the center of the target at mean energy.

Meson Energy (Mev)	Decay in Flight	Multiple Scattering	Nuclear Interaction	
			H	D
18	0.932	1.000	1.000	0.999
21	0.940	0.966	0.998	0.997
24	0.946	0.984	0.995	0.994
29	0.954	0.969	0.990	0.988
37	0.964	0.961	0.978	0.976
51	0.973	0.933	0.949	0.946
57	0.976	0.927	0.933	0.930
63	0.980	0.909	0.915	0.912
68	0.984	0.894	0.896	0.893
74	0.989	0.893	0.876	0.873
79	0.994	0.885	0.855	0.851
84	1.000	0.892	0.833	0.829
91	1.000	0.891	0.810	0.806
93	1.000	0.938	0.792	0.788

second.[44] Using time dilation and the relativistic equation for total energy, we find that the time of transit in the meson frame between points a and b in the laboratory frame becomes

$$t = \frac{E_o}{c} \int_a^b \frac{dx}{\sqrt{T(T+2E_o)}} ,$$

where E_o = rest energy of the π mesons,

T = kinetic energy of the π meson.

This formula can be written

$$t = \frac{E_o}{c} \sum \frac{\Delta x_i}{\sqrt{T_i(T_i+2E_o)}} ,$$

where the Δx_i's extend from a to b and the change in T is small over each Δx_i. This formula was used to determine t and thus the decay correction. The calculation was done by dividing the front part of the target, the absorbers, and the first scintillator into small segments and considering the air path as one segment.

Some of the μ-mesons from the decay of the π-mesons of all energies get to the scintillator and decay. At 143° this correction was calculated. It was a 1% correction at the low energies and 3% at the high energies. The decay-in-flight correction listed in Table III includes a correction for this effect. The μ-meson contribution correction was neglected at 180°. A detailed calculation at 180° of this effect would be greatly complicated by the magnetic field; however, a comparison of the 180° and the 143° geometries indicated that the μ contribution would be smaller at 180° than at 143°. In addition, the calibration emulsions were not subject to this effect; consequently, only the relative change with energy is important. The correction for μ contribution at 180° is therefore negligible.

2. Nuclear Interaction

Mesons are lost before reaching the detector by interaction in the target, the absorbers, and the first scintillator. The number reaching the detector is given by $e^{-\Sigma N\sigma\Delta x}$,

where N = atoms per cm^3 of the material the meson is passing through,

Δx = thickness of segment of the material,

σ = cross section for interaction in that segment.

The segments had to be kept small, as σ varies with energy. The σ's for π^+ in carbon and copper were those of Stork.[45] The σ's for π^+ in hydrogen were based on the work of several authors.[46-49] The σ's for π^+ in helium were taken as a straight line through the one π^+ point of Fowler et al.[46] with the same slope as the two π^- points of the same authors. The σ's for deuterium were based on the same data as for hydrogen. The values used were the sum of the σ's for π^+ on p and π^- on p. The assumption was made that π^- on p is the same as π^- on n, which appears to be a fairly reasonable assumption if Coulomb effects are neglected.

3. Multiple Scattering in the Absorbers

Many workers have calculated this type of multiple-scattering correction; therefore it is not presented in detail here. (See References 50-52). The calculations are based on the work of Eyges[53] and Foldy.[54]

A gaussian distribution function results with rms displacement

$$\sigma = \sqrt{2\,(A_2^2 + 2LA_1 + L^2A_o)}$$

where L = the distance from the absorber to the detector,

$$A_n = \int_o^t \frac{(t-\eta)^n}{w^2(\eta)}\, d\eta,$$

$$w = 2\, v\, P/E_s\ ,$$

v = velocity of meson,

P = momentum of meson,

E_s = 21.2 Mev,

t = distance in radiation lengths of absorber material,

η = integration variable in radiation lengths of absorber material.

The A's were calculated by numerical integration. The calculation of the actual correction consisted of dividing the channel into segments in both vertical and horizontal directions. Then the fraction of mesons from each segment that passed through the detector was calculated. This fraction was $\mathrm{erf}\,\frac{(w/2-x)}{\sigma} + \mathrm{erf}\,\frac{(w/2+x)}{\sigma}$, where w is width of detector and x is the distance of the center of the segment from the center of the channel. These fractions were summed and normalized for the

number of segments in order to find the correction for one direction. The product of the two directions gave the total correction.

4. Other Corrections

Several other corrections were considered, but all appeared to be small. One of these was the change in counting efficiency of the β's at 180° because of the change in magnetic field. At high magnetic fields the radius of curvature of the β is smaller than at normal fields; therefore, β-particles near the edge of the scintillator have a higher probability of being counted than they would have at low magnetic fields. This efficiency change was calculated, using both curvature and scattering in the magnetic field, and was found to be negligible.

Another correction to be considered is multiple scattering in the channel and the target walls. This correction is believed to be very small. The effect is largest for particles incident to and leaving the walls at small angles. The emulsion area scanned was small and far away from the channel walls. Thus the correction to the emulsion data should be negligible. The scintillators were smaller than the channel, but were not as far away from the channel walls as was the emulsion. Since emulsions were used to calibrate the counters, the wall scattering would be automatically compensated for at the calibration energy and the correction would be reduced to its variation with energy. This scattering correction is expected to be small. A Monte Carlo type calculation is planned for the future when calculator time becomes available.

C. Calculation of Energies

The energies were calculated using range-energy curves for the π-meson that were derived from the range-energy curves of Aron, Hoffman, and Williams[55] using

$$R_{meson}(E) = \frac{m_\pi}{M_p} R_{proton}\left(\frac{M_p E}{m_\pi}\right),$$

where R's are ranges, m's are masses, and E is the meson energy. Here $m_\pi = 273.3$.[56] The ranges in various materials were employed to calculate the energy of the mesons which originated in various parts of the target and which stopped in various positions in the detector.

With the gas target at 180° the energy resolution was quite poor, owing to the long target. There was also a tendency to favor the lower energies, since the meson contribution was larger from the end of the target nearer the detector. The meson energy increases along the target from the near to the far end. The solid angle subtended by the detectors decreases, whereas the decay-in-flight and the nuclear-absorption corrections increase with target position from the near to the far end. The mean energies were calculated by weighting the energies by the three factors just mentioned and averaging over the target length. This method gave a mean energy corresponding to the energy of a meson originating 10 inches from the detector end of the target. The entire width of the meson energy distribution due to this target was 23 Mev at the lowest energy and 15 Mev at the highest energy. The energy-resolution curve is shown in Fig. 18.

The other targets were relatively thin; therefore, the mean energy used is the energy of a meson originating at the center of the target and stopping in the middle of the detector. The energy width of the carbon target varied from 5 Mev at low energies to 3 Mev at high energies. The liquid-target energy width varied from 7 to 3 Mev.

The energy width of the scintillation detector varied from 13 Mev to 5 Mev at 143° and from 8 to 5 Mev at 180°. The energy width of the areas of emulsions scanned was about 8 Mev.

D. Calculation of Cross Sections

Two types of cross section were calculated. They might be termed the first and second differential cross sections (i.e., $d\sigma/d\Omega$ and $d^2\sigma/dEd\Omega$). Since the first differential cross sections were calculated from the second differential cross sections, the second differential cross sections are considered first.

1. The Second Differential Cross Section

The second differential cross section is given basically by

$$\frac{d^2\sigma}{dEd\Omega} = \frac{N}{n \frac{\Delta Q}{\Delta C} \varepsilon w h \Delta R \int_0^t \frac{d\Omega}{dA} \frac{dE}{dR} dt}$$

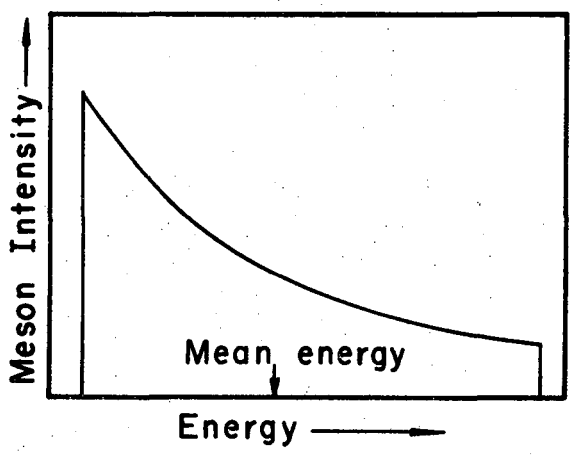

MUL-909

Fig. 18. Energy-resolution curve for the gas target.

where N = mesons per unit of integrated photon beam,

$\mathcal{E}$ = efficiency,

n = protons per cm^3,

$\frac{\Delta Q}{\Delta C}$ = equivalent quanta per unit of integrated beam,

w = width of detector in cm,

h = height of detector in cm,

ΔR = depth of detector in cm,

t = thickness of target in cm,

$\frac{d\Omega}{dA}$ = solid angle subtended at a position in the target by the detector in units of $1/cm^2$,

$\frac{dE}{dR}$ = energy spread of meson leaving a point in the target per spread in range of the mesons at the detector in units of Mev/cm.

a. <u>From 180° Data.</u> At 180° the basic formula was modified to the form

$$\frac{d^2\sigma}{dEd\Omega} = \frac{N}{n\,\frac{\Delta Q}{\Delta C}\;\mathcal{E}\,\Delta R\,w\,h\,\Delta t\,\sum \frac{d\Omega}{dA}\;\frac{dE}{dR}},$$

where t = the thickness of a segment of the target in cm. The summation is over the segments into which the target is divided.

(1) Emulsions. For the emulsion, the efficiency, $\mathcal{E}$, was nearly one; therefore, absolute values could be calculated. The number of mesons found was corrected for decay in flight, nuclear absorption, and empty-target background. The empty-target correction was determined by the counter data. The volume scanned was corrected for shrinkage. The resulting number was the corrected number of π-mesons detected per unit of integrated beam per unit volume of emulsion. This is $N/wh\Delta R$ in the above formula. The number of protons per cm^3, n, was determined from the temperature and pressure, from the data of Johnston et al.[57] The Cornell calibration of the beam mentioned in section II, B, 6 was $\frac{\Delta Q}{\Delta C}$, which is given in units of equivalent quanta per unit of integrated beam. The equivalent quantum is the total energy in the beam divided by the maximum energy of the bremsstrahlung. The target was divided into 8 segments with t = 3 inches = 7.62 cm.

$$\frac{d\Omega}{dA} = \frac{1}{(A + \rho\,\phi)\left[\rho \operatorname{Sin}\phi + A \operatorname{Cos}\phi\right]}$$

where A = distance from target to edge of pole tip in cm,

ρ = radius of meson channel in cm,

ϕ = central angle subtended by channel from the edge of the pole tip to the center of the detector.

(See Reference 58, Appendix A, for derivation.)

Particle trajectory measurements by the current-carrying-wire method have shown that the above formula is applicable because the target was placed in a magnetic shield. The fringing field at the target was small. The remaining term dE/dR is defined above and is determined from the energy resolution of the detector (Section III, C).

(2) Counters. For the counters at 180° the basic formula may be written

$$\frac{d^2\sigma}{dE\,d\Omega} = \frac{1}{n\frac{\Delta Q}{\Delta C}\,\varepsilon\, w\, h\, \Delta t}\;\frac{N}{\sum \frac{d\Omega}{dA}\,\Delta E} = C\;\frac{N}{\frac{d\Omega}{dA}\,\Delta A}$$

where ΔE = the energy width of the detector for a particle originating at a given point in the target,

$C = \dfrac{1}{n\frac{\Delta Q}{\Delta C}\,\varepsilon\, w\, h\, \Delta t}$, which is a constant for all meson energies with a given target material.

Comparing the cross section formula for counters and emulsion, we find that

$$C = \frac{(d^2\sigma/dE\,d\Omega)\,\text{emulsion}}{(N/\,\Sigma(d\Omega/dA)\,\Delta E)\,\text{counters}}$$

at the calibration energy with the same target material (hydrogen). The N, here, has been corrected for decay in flight, nuclear interaction, multiple scattering in absorbers, accidental coincidence background, and empty target background. For other target materials it is immediately seen that

$$C' = \frac{n}{n'}\,C$$

if the geometry is not changed. (Primes refer to new target material.) With the carbon target,

$$C' = \frac{\Delta t}{\Delta t'}\,\frac{n}{n'}\,C\,,$$

since the target thickness was different. The values of the n's for hydrogen and deuterium are from Reference 57; the values for helium are from Reference 50. The second differential cross section for the counter data and the appropriate constant is obtained using

$$N\left(\sum \frac{d\Omega}{dA}\ \Delta E\right)\text{, and the appropriate constant.}$$

b. <u>From 143° Data</u>

At 143° the calculation was similar to 180°, but the summation over the target was not required as the target was relatively thin. For emulsions and counters, the basic formulas become, respectively,

$$\frac{d^2\sigma}{dEd\Omega} = \frac{r^2}{n\frac{\Delta Q}{\Delta C}\,\varepsilon\,\frac{dE}{dR}\,t}\ \frac{N}{wh\Delta R}\,, \qquad \text{(emulsions)}$$

$$\frac{d^2\sigma}{dEd\Omega} = \frac{r^2}{n\frac{\Delta Q}{\Delta C}\,\varepsilon\,wht}\ \frac{N}{\Delta E} = C\,\frac{N}{\Delta E}\,, \qquad \text{(counters)}$$

where $C = \dfrac{(d^2\sigma/dEd\Omega)\ \text{emulsion}}{(N/\Delta E)\ \text{counters}}$ at same energy and target,

r = distance from target center to detector center,

t = weighted mean thickness of target.

Here $\frac{d\Omega}{dA}$ has been replaced with $1/r^2$ since there is no magnetic field, and again

$$C' = \frac{n}{n'}\,C.$$

Two emulsion points were obtained in the counter-data range so that two values of C were calculated. The counter data were fitted to these points.

The weighted mean value of t was obtained by weighting the target thickness at each point in the photon beam by the beam intensity at that point and integrating over the beam areas. The angular distribution of the photon beam used for this calculation was measured by Anderson, Kenney, and McDonald.[39] The values of n for liquid hydrogen and deuterium were calculated from the densities[59] of liquid hydrogen and deuterium at the liquid hydrogen boiling point. Other values in the formula were obtained by the method described in the 180° section.

2. The First Differential Cross Section

The basic formula for the differential cross section in the laboratory system at a given photon energy is

$$\left(\frac{d\sigma}{d\Omega}\right)_{lab} = \frac{N}{n\frac{\Delta Q}{\Delta C}\,\varepsilon\, wh\Delta R\,\frac{ko}{area}\int_0^t \frac{d\Omega}{dA}\,\frac{dk}{dE}\,\frac{dE}{dR}\,\frac{f(k)}{k}\,dt},$$

where ko = maximum energy of bremsstrahlung beam in Mev (342),

$area$ = the area under the bremsstrahlung curve, (in arbitrary units x Mev)

$\frac{dk}{dE}$ = the rate of change of photon energy with meson energy,

k = energy of the photon producing the meson of energy E in the target,

$f(k)$ = ordinate of bremsstrahlung curve, i.e. number of photons of energy k x k, in arbitrary units.

All other quantities are the same as previously defined. These formulas become, at 180° and 143° respectively,

$$\left(\frac{d\sigma}{d\Omega}\right)_{lab} = \frac{N}{n\frac{\Delta Q}{\Delta C}\,\varepsilon\, wh\Delta t\,\frac{ko}{area}\sum\frac{d\Omega}{dA}\,\Delta E\,\frac{dk}{dE}\,\frac{f(k)}{k}},$$

$$\left(\frac{d\sigma}{d\Omega}\right)_{lab} = \frac{r^2}{n\frac{\Delta Q}{\Delta C}\,\varepsilon\, wht\,\frac{ko}{area}}\;\frac{N}{\frac{dk}{dE}\,\frac{f(k)}{k}\,\Delta E}$$

If these formulas are compared with the second differential cross sections, it follows immediately, for 180° and 143° respectively, that

$$\left(\frac{d\sigma}{d\Omega}\right)_{lab} = \frac{area}{ko}\;\frac{\sum\frac{d\Omega}{dA}\,\Delta E}{\sum\frac{d\Omega}{dA}\,\Delta E\,\frac{dk}{dE}\,\frac{f(k)}{k}}\;\frac{d^2\sigma}{dEd\Omega}$$

$$\left(\frac{d\sigma}{d\Omega}\right)_{lab} = \frac{1}{\frac{ko}{area}\,\frac{dk}{dE}\,\frac{f(k)}{k}}\;\frac{d^2\sigma}{dEd\Omega}$$

Since they require that the photon energy be known, these formulas are used with hydrogen only. In the two-body reaction $\gamma + p \longrightarrow \pi^+ + n$, conservation of momentum and energy allow k to be calculated from E.

The value dk/dE is also calculable from the above relations. The quantities f(k) and area are determined from the bremsstrahlung curve calculated by Terwilliger and Jones.[60] The center-of-mass cross sections $(d\sigma/d\Omega)_{c.m.}$ were calculated using the transformations of Malmberg and Koester.[61]

IV. RESULTS

A. 180° Position

1. $d^2\sigma/dEd\Omega$ for Hydrogen, Deuterium, Helium, and Carbon

The $d^2\sigma/dEd\Omega$ for π^+-mesons from hydrogen, deuterium, helium, and carbon were calculated as described in section III, D, 1. The results are given in Table IV. The errors shown are standard deviations of the relative errors only. They do not include the 10% error in the absolute monitoring of the beam. The absolute value of the carbon data is probably good to only 30%. The absolute calibration of the carbon data depended on the fact that the efficiency of the scintillation counters had to remain constant while solid targets were removed and the gas target was set up. Approximately a day elapsed from the time the standard point on solid targets was run until the time the standard point was run on the gas target. The $d^2\sigma/dEd\Omega$ for hydrogen from the CH_2-C data agreed reasonably well with the gas-target data but the statistics were poor. Figures 19 to 22 show the energy distributions at 180°.

2. Deuterium-Hydrogen, Helium-Hydrogen, and Carbon-Hydrogen Ratios

Ratios of the second differential cross section for π^+-mesons from deuterium, helium, and carbon to the second differential cross section for hydrogen are given in Table V and Fig. 23. The data are presented in this manner since the photon energy responsible for the reaction is not known for D, He, and C.

The carbon-hydrogen ratios were taken from the C - CH_2 subtraction and do not depend on the efficiency's being constant as described above.

3. $d\sigma/d\Omega$ for Hydrogen

The differential cross sections for π^+-mesons from hydrogen at 180° are given in Table VI. Both the laboratory and the center-of-mass

Table IV

$d^2\sigma/dEd\Omega$ at 180° for π^+-mesons from hydrogen, deuterium, helium and carbon. The errors given are standard deviations and do not include the error of absolute calibration. The numbers given in the body of the table have units of

$$\frac{cm^2}{\text{Mev Steradian Proton Equivalent Quantum}}$$

Mean Meson Energy (Mev)	$d^2\sigma/dEd\Omega$			Mean Meson Energy (Mev)	$d^2\sigma/dEd\Omega$
	Hydrogen	Deuterium	Helium		Carbon
	$\times 10^{-32}$	$\times 10^{-32}$	$\times 10^{-32}$		$\times 10^{-32}$
34	4.63 ± 0.44	5.25 ± 0.29	3.80 ± 0.47	25	3.49 ± 0.22
38	5.18 ± 0.36	4.65 ± 0.26		30	2.89 ± 0.19
42	5.20 ± 0.27	5.64 ± 0.29	2.92 ± 0.40	39	3.30 ± 0.21
47	6.94 ± 0.16	6.22 ± 0.23		47	3.69 ± 0.23
50	6.19 ± 0.27	5.70 ± 0.25	3.42 ± 0.34	56	3.47 ± 0.20
54	5.79 ± 0.26	5.82 ± 0.29		66	3.05 ± 0.20
57	4.59 ± 0.25	4.81 ± 0.29	2.52 ± 0.34	75	1.94 ± 0.21
63	3.45 ± 0.22	4.29 ± 0.29	2.40 ± 0.34	85	1.13 ± 0.15
68	2.68 ± 0.24	3.09 ± 0.29	1.06 ± 0.31		
72	1.57 ± 0.20	2.42 ± 0.25			
76		2.08 ± 0.29	2.27 ± 0.32		
81	0.41 ± 0.22	1.27 ± 0.25			

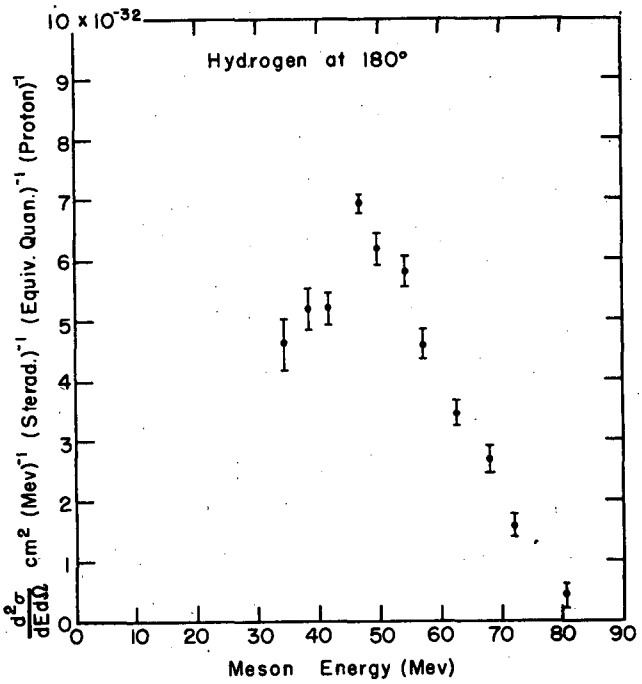

MUL-861

Fig. 19. Energy distribution of π^+-mesons from hydrogen at 180°. Errors shown are standard deviations and do not include error in absolute calibration of the beam.

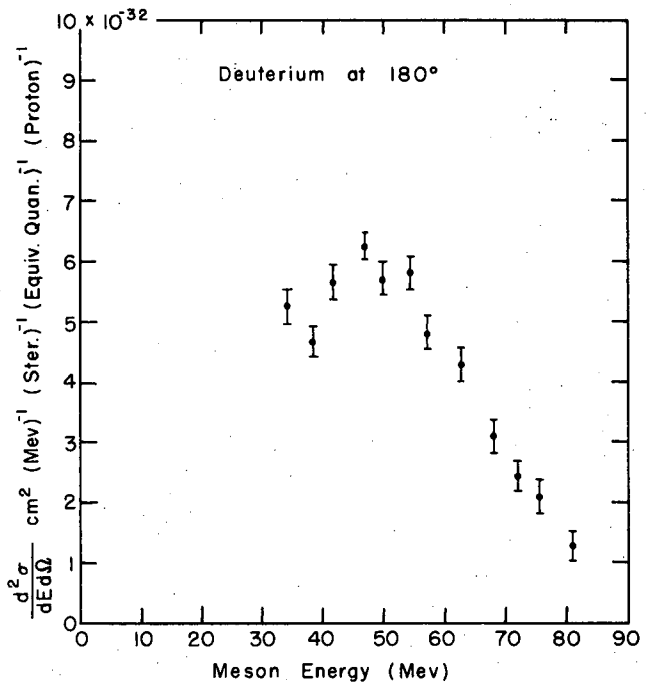

MUL-872

Fig. 20. Energy distribution of π^+-mesons from deuterium at 180°. Errors shown are standard deviations and do not include error in absolute calibration of the beam.

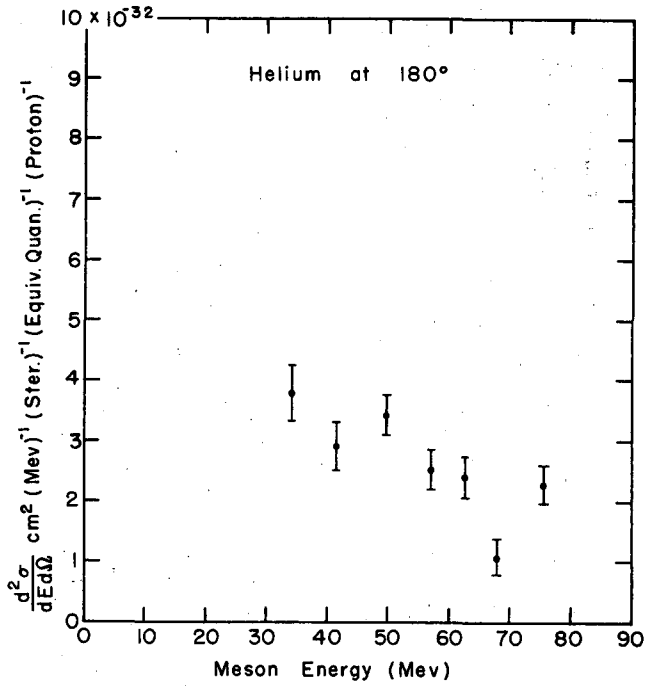

MUL-871

Fig. 21. Energy distribution of π^+-mesons from helium at 180°. Errors shown are standard deviations and do not include error in absolute calibration of the beam.

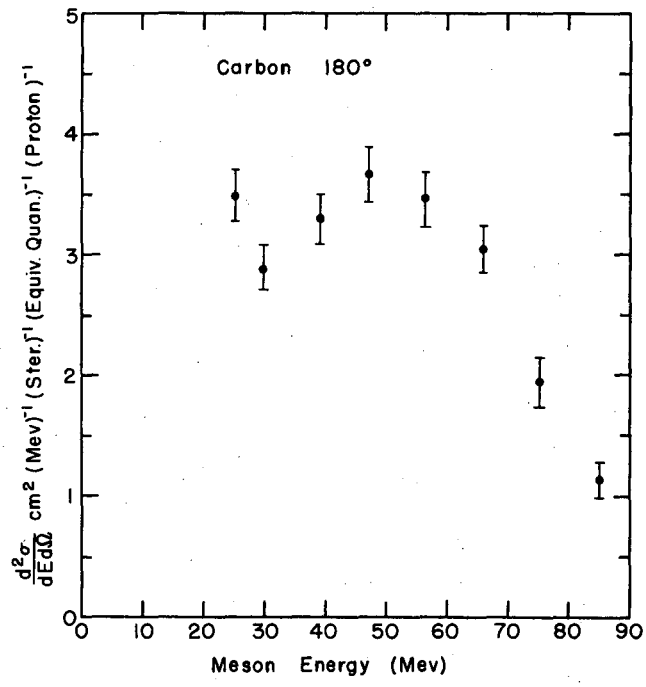

MUL-856

Fig. 22. Energy distribution of π^+-mesons from carbon at 180°. Errors shown are standard deviations and do not include error in absolute calibration of the beam.

Table V

$$\frac{\left(\frac{d^2\sigma}{dEd\Omega}\right)_{D,\,He,\,C}}{\left(\frac{d^2\sigma}{dEd\Omega}\right)_{H}} \quad \text{Ratios at } 180^{\circ}$$

Errors are standard deviations

Mean Meson Energy (Mev)	D/H	He/H	Mean Meson Energy (Mev)	C/H
34	1.124 ± 0.113	0.82 ± 0.13	25	0.78 ± 0.15
38	0.877 ± 0.077		30	0.454 ± 0.066
42	1.063 ± 0.077	0.562 ± 0.084	39	0.453 ± 0.061
47	0.875 ± 0.038		47	0.522 ± 0.079
50	0.897 ± 0.056	0.554 ± 0.058	56	0.346 ± 0.043
54	0.974 ± 0.065		66	1.12 ± 0.35
57	1.011 ± 0.083	0.549 ± 0.080	75	0.85 ± 0.36
63	1.21 ± 0.11	0.69 ± 0.11		
72	1.51 ± 0.25			
81	3.1 ± 1.8			

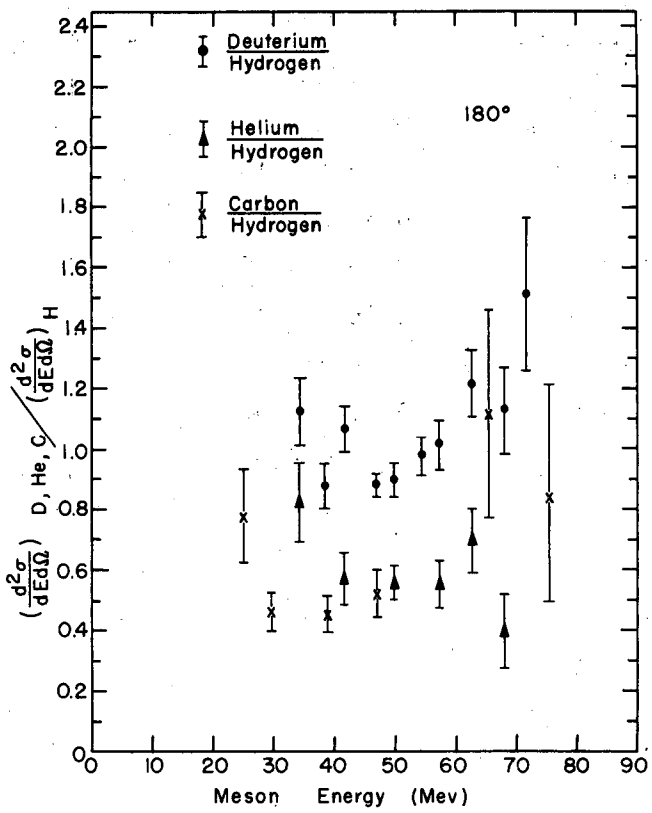

MUL-867

Fig. 23. Deuterium-hydrogen, helium-hydrogen, and carbon-hydrogen ratios for π^+-mesons at 180°. Standard deviations are shown. The ratios are per proton.

Table VI

Differential cross sections for π^+-mesons at 180° from hydrogen. Standard deviations are shown, which do not include error in absolute calibration.

Mean Meson Energy (Mev)	Mean Photon Energy (Mev)	$(d\sigma/d\Omega)_{lab}$ $\frac{cm^2}{\text{Steradian Proton Photon}}$	$(d\sigma/d\Omega)_{c.m.}$ $\frac{cm^2}{\text{Steradian Proton Photon}}$
		$\times 10^{-30}$	$\times 10^{-30}$
34	237	5.07 ± 0.44	9.49 ± 0.82
38	246	5.88 ± 0.40	10.99 ± 0.75
42	252	6.00 ± 0.33	11.24 ± 0.62
47	268	8.33 ± 0.20	15.66 ± 0.38
50	276	7.56 ± 0.33	14.26 ± 0.62
54	288	7.30 ± 0.35	13.88 ± 0.67
57	296	5.98 ± 0.33	11.41 ± 0.63
63	311	5.26 ± 0.33	10.13 ± 0.64

cross sections are shown. The errors are standard deviations and do not include absolute calibration error. Figure 24 shows the excitation function at 180°. Two more points were obtained, but are not shown because they fall on the steep part of the bremsstrahlung just before cut-off. The absolute values of these points are extremely sensitive to a slight variation in maximum photon energy; these points are experimentally slightly higher than the extrapolated curve through the other points. This fact suggests that the maximum energy is slightly low. The 143° data also confirm this result and the result is in agreement with the value $k_{max} = 342 \pm 6$ Mev of Anderson, Kenney, and McDonald[39] rather than the old value of 322 ± 6 Mev.[38]

B. 143° Position

1. $d^2\sigma/dEd\Omega$ for Hydrogen and Deuterium

The $d^2\sigma/dEd\Omega$ for π^+-mesons from hydrogen at 143° and deuterium are shown in Table VII. Standard deviations are shown which do not include the error in the absolute calibration. Figures 25 and 26 show the energy distribution for π^+-mesons at 143°.

2. Deuterium-Hydrogen Ratios

Table VII and Fig. 27 give the ratio

$$\frac{\left(\frac{d^2\sigma}{dEd\Omega}\right)_D}{\left(\frac{d^2\sigma}{dEd\Omega}\right)_H}$$

for π^+-mesons.

3. π^-/π^+ Ratio from Deuterium

When the calibration emulsions were scanned at 143° the σ endings were recorded. A π^-/π^+ ratio was calculated using

$$\frac{\pi^-}{\pi^+} = \frac{1.37\sigma}{\pi-\mu}$$

The 1.37 comes from the fact that the zero-prong stars are not seen. This result was determined by Adelman and Jones.[63] The π^-/π^+ ratios were 1.18 ± 0.24 at 13 Mev, 1.19 ± 0.25 at 25 Mev, and 1.41 ± 0.24 at 40 Mev.

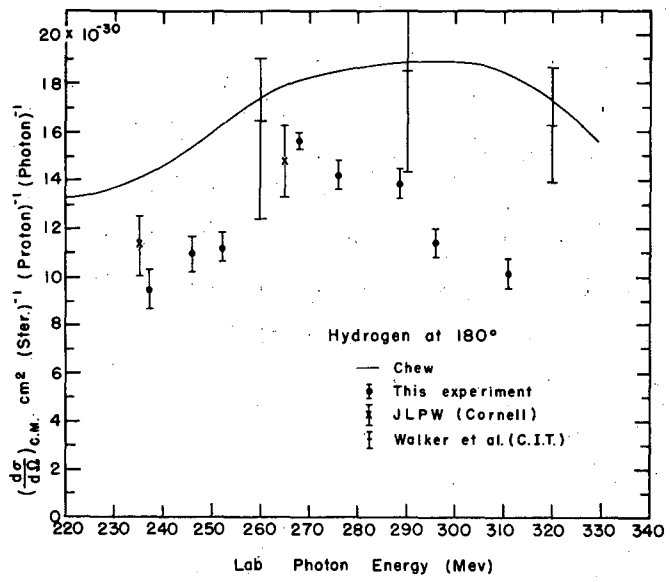

MUL-906

Fig. 24. Excitation function for π^+-mesons from hydrogen at 180°. Standard deviations are shown. The curve is from Chew's cutoff theory.[62] Three points from Walker et al.[22] and two points from Jenkins et al.[26] are shown.

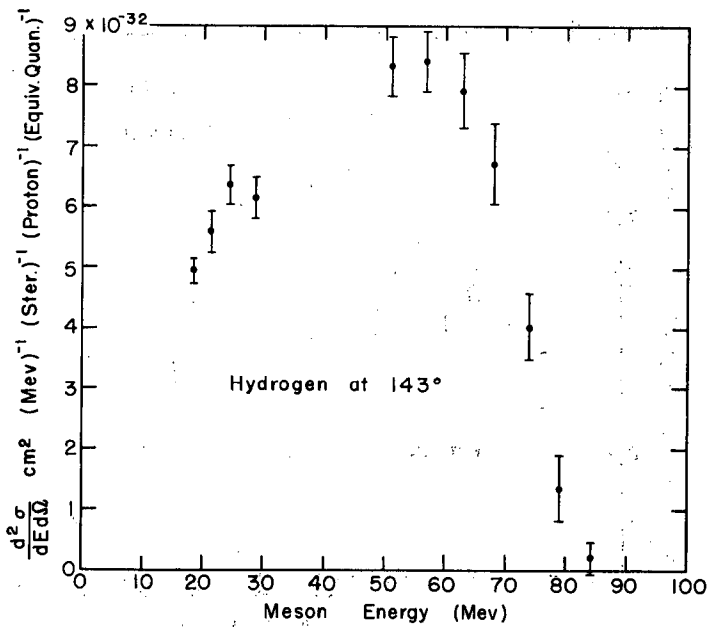

MUL-869

Fig. 25. Energy distribution of π^+-mesons from hydrogen at 143°. Errors shown are standard deviations and do not include error in absolute calibration of the beam.

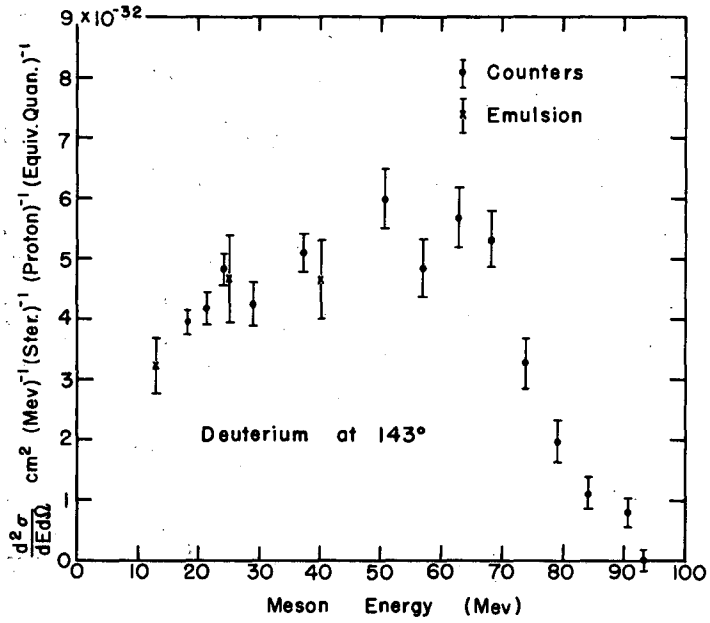

MUL-870

Fig. 26. Energy distribution of π^+-mesons from deuterium at 143°. Errors shown are standard deviations and do not include error in absolute calibration.

Table VII

$\frac{d^2\sigma}{dEd\Omega}$ at 143° for π^+-mesons from hydrogen and deuterium, and deuterium - hydrogen ratio.

Standard deviations are shown and do not include the error in absolute calibration.

Mean Meson Energy (Mev)	$d^2\sigma/dEd\Omega$ $\frac{Cm^2}{\text{Mev Steradian Proton Equivalent Quantum}}$		$\frac{(d^2\sigma/dEd\Omega)_D}{(d^2\sigma/dEd\Omega)_H}$
	Hydrogen	Deuterium	
	x 10^{-32}	x 10^{-32}	
13*		3.23 ± 0.46	
18	4.95 ± 0.21	3.98 ± 0.20	0.811 ± 0.053
21	5.58 ± 0.34	4.16 ± 0.27	0.753 ± 0.067
24	6.38 ± 0.33	4.83 ± 0.27	0.764 ± 0.058
25*		4.67 ± 0.73	
29	6.14 ± 0.35	4.25 ± 0.38	0.699 ± 0.074
37		5.09 ± 0.33	
40*		4.63 ± 0.64	
51	8.35 ± 0.50	5.98 ± 0.50	0.724 ± 0.075
57	8.45 ± 0.49	4.84 ± 0.47	0.572 ± 0.065
63	7.97 ± 0.62	5.65 ± 0.49	0.709 ± 0.083
68	6.73 ± 0.67	5.32 ± 0.47	0.786 ± 0.105
74	4.02 ± 0.55	3.27 ± 0.42	0.82 ± 0.15
79	1.35 ± 0.55	1.97 ± 0.34	1.47 ± 0.65
84	0.21 ± 0.26	1.10 ± 0.27	5.46 ± 0.69
91		0.80 ± 0.25	
93		0.0 ± 0.19	

*Indicates emulsion point

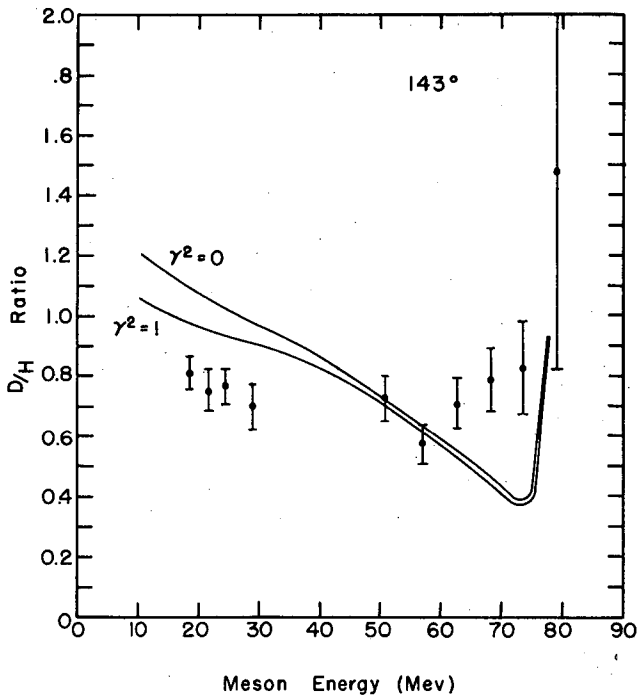

MUL-868

Fig. 27. Deuterium-hydrogen ratio for π^+-mesons at 143°. Standard deviations are given. The curves are from a phenomenological theory of Chew and Lewis.[64] The $\gamma^2 = 0$ is the all-spin interaction case and $\gamma^2 = 1$ is the no-spin interaction case.

4. $d\sigma/d\Omega$ for Hydrogen

The differential cross sections for π^+-mesons at 143° laboratory angle are given in Table VIII. Both laboratory and center-of-mass cross sections are given. Standard deviations are given which do not include the error for absolute calibration. The center-of-mass angle for all these points is between 153° and 152°. Figure 28 shows the excitation function for 143° laboratory angle.

V. DISCUSSION

The π^+-meson from hydrogen results are compared with other experiments in Fig. 24 and 28 - 34. Data from Cornell, Illinois, and California Institute of Technology are shown.[21, 22, 24, 26, 27, 30] The agreement appears to be good.

The hydrogen data have been compared with the theory of Chew.[65] This theory uses a moderately weak coupling and has two arbitrary parameters. These parameters are the coupling constant for the meson field to the nucleon, and the energy cutoff. The nucleon is considered as a finite source in phase space and it is normalized by integrating a source function over phase space. Chew has used a step function for this source function, which is zero for values greater than a certain energy value. This energy value is the energy-cutoff parameter. The theory is limited in that S-wave meson-nucleon scattering has been neglected. (Only P-wave scattering phase shifts are used.) In the curves shown the two arbitrary parameters were determined from the P-wave phase shifts of the π-meson-nucleon scattering experiments.

The formula[62] used to calculate the differential cross sections from Chew's theory is

$$\left(\frac{d\sigma}{d\Omega}\right)_+ = \frac{2e^2f^2}{\mu^2}\,\frac{q/\nu}{(1+\frac{\nu}{M})}\left\{(1-\frac{\omega}{2M})^2 - \frac{\mu^2}{2\omega^2}\,\frac{v^2\sin^2\theta}{(1-v\cos\theta)^2} + \right.$$

$$|M_1-E_2|^2\cos^2\theta - 2\mathrm{Re}\,(M_1-E_2)\left(1-\frac{\frac{v^2}{2}\sin^2\theta}{1-v\cos\theta}\right)\cos\theta + \left[2\,|M_1|^2 + \right.$$

$$\left.\left. 1/2\,|M_1+E_2|^2 + v\,\mathrm{Re}(M_1+E_2)\right]\sin^2\theta\right\},$$

Table VIII

Differential cross sections for π^+-mesons at 143° laboratory angle or 152° - 153° center-of-mass angle from hydrogen.

Standard deviations are shown, which do not include error in absolute calibration.

Mean Meson Energy (Mev)	Mean Photon Energy (Mev)	$(d\sigma/d\Omega)_{lab}$ $\frac{cm^2}{\text{Steradian Proton Photon}}$	$(d\sigma/d\Omega)_{c.m.}$ $\frac{cm^2}{\text{Steradian Proton Photon}}$
		$\times 10^{-30}$	$\times 10^{-30}$
18	196	5.12 ± 0.22	9.00 ± 0.39
21	203	5.97 ± 0.36	10.28 ± 0.62
24	209	7.04 ± 0.36	11.99 ± 0.61
29	219	7.02 ± 0.40	11.83 ± 0.67
51	267	10.99 ± 0.65	18.49 ± 1.10
57	282	11.48 ± 0.66	19.45 ± 1.13
63	296	11.21 ± 0.87	19.15 ± 1.50
68	310	10.07 ± 1.01	17.36 ± 1.75
74	325	7.81 ± 1.06	13.60 ± 1.85

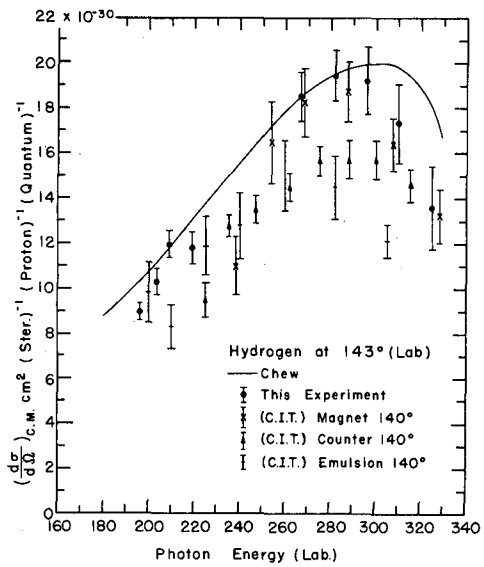

MUL-905

Fig. 28. Excitation function for π^+-mesons from hydrogen at 143°. Standard deviations are shown. The curve is from Chew's cutoff theory.[62] Points obtained at the California Institute of Technology at 140° are also shown.[21, 22, 30]

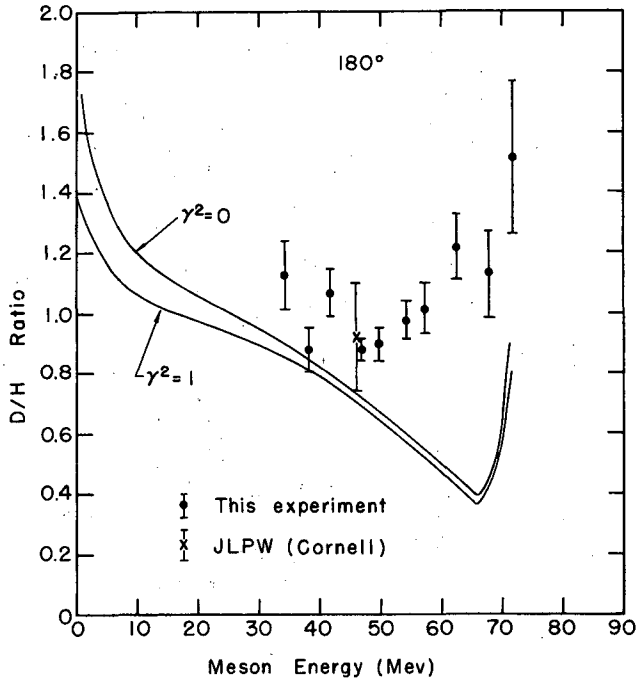

MUL-873

Fig. 29. Deuterium-hydrogen ratio for π^+-mesons at 180°. Standard deviations are given. The curves are from a phenomenological theory of Chew and Lewis. The $\gamma^2 = 0$ is the all-spin interaction case and $\gamma^2 = 1$ is the no-spin interaction case. A point obtained by Jenkins et al.[26] (JLPW Cornell) is shown.

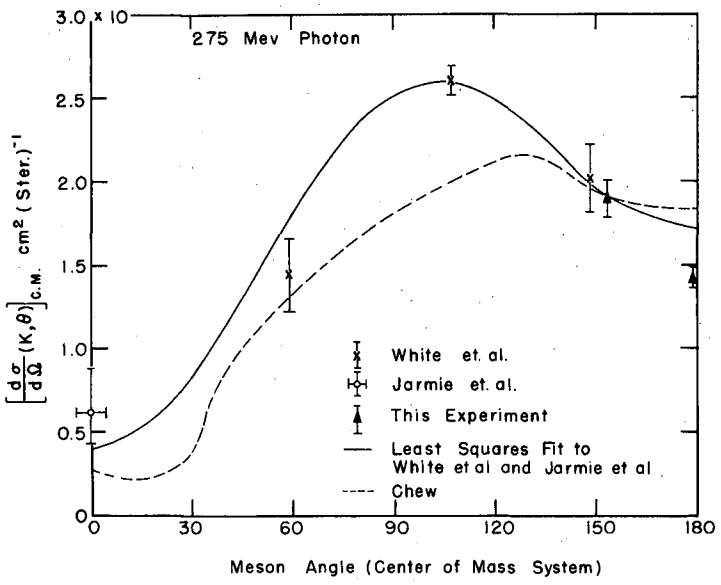

MUL-858

Fig. 30. Angular distribution for π^+-mesons from hydrogen for 275-Mev photons. Standard deviations are shown. Points from White et al.[16] and Jarmie et al.[19] are shown. Solid curve is a least-squares fit of A+B cos θ + C $\sin^2 \theta$ to the White and Jarmie data. The broken curve is from Chew's[62] cutoff theory.

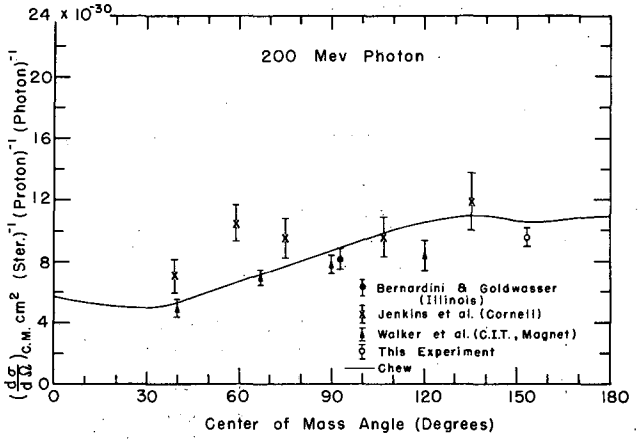

MUL-907

Fig. 31. Angular distribution for π^+-mesons from hydrogen for 200-Mev photons. The data of Bernardini and Goldwasser (Illinois),[24] Jenkins et al. (Cornell),[26] Walker et al. (C.I.T., Magnet),[22] and this experiment are shown. The curve is from Chew's cutoff theory.[62]

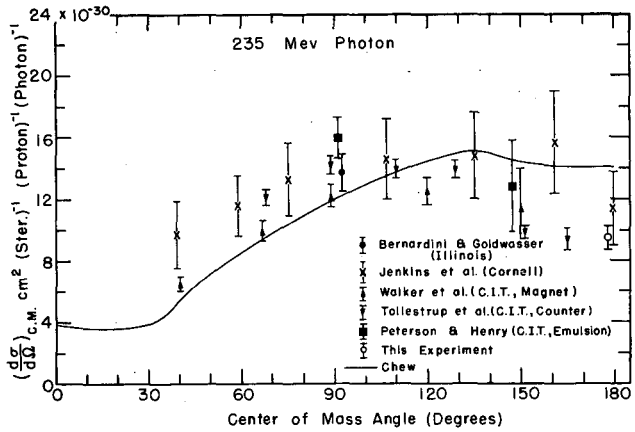

MUL-908

Fig. 32. Angular distribution for π^+-mesons from hydrogen for 235-Mev photons. The data of Bernardini and Goldwasser (Illinois),[24] Jenkins et al. (Cornell),[26] Walker et al. (C. I. T., Magnet),[22] Tollestrup et al. (C. I. T., Counter),[21] Peterson and Henry (C. I. T., Emulsion),[30] and this experiment are shown. The curve is from Chew's cutoff theory.[62]

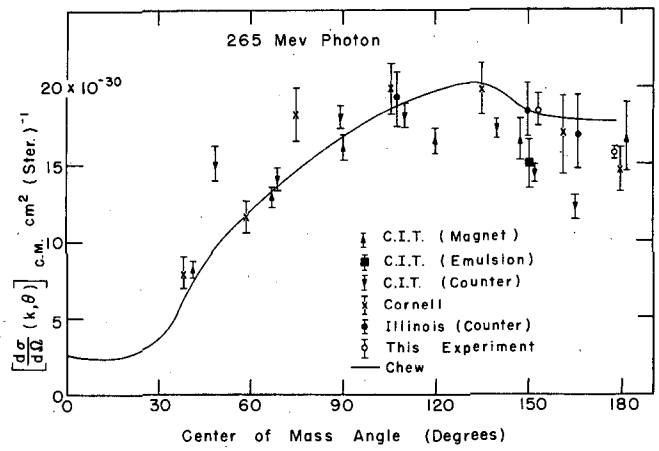

MUL-903

Fig. 33. Angular distribution for π^+-mesons from hydrogen for 265-Mev photons. The data of Walker et al. (C. I. T., Magnet),[22] Tollestrup et al. (C. I. T., Counter),[21] Peterson and Henry (C. I. T., Emulsion),[30] Jenkins et al. (Cornell),[26] Leiss and Robinson (Illinois Counter),[27] and this experiment are shown. The curve is from Chew's cutoff theory.[62]

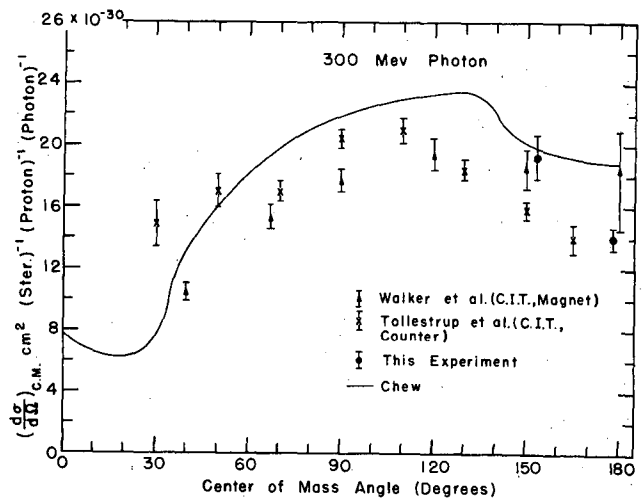

MUL-904

Fig. 34. Angular distribution for π^+-mesons from hydrogen for 300-Mev photons. The data of Walker et al. (C.I.T., Magnet),[22] Tollestrup et al. (C.I.T., Counter),[21] and this experiment are shown. The curve is from Chew's cutoff theory.[62]

where all momenta and energies are in the center-of-mass system, and mass and momentum are in Mev;

e = charge of the electron, $e^2 = 1/137$;

f = coupling constant, $f^2 = 0.073$;

μ = π meson mass;

M = proton mass;

ν = photon center-of-mass energy;

$\omega = \sqrt{1 + q^2}$;

q = π-meson momentum;

v = meson velocity in units of c;

$M_1 = m_1 (\mu\nu/q^2) e^{i\delta_{33}} \sin \delta_{33}$;

$E_2 = e_2 (\mu\nu/q^2) e^{i\delta_{33}} \sin \delta_{33}$;

δ_{33} = meson-nucleon scattering phase shift for the 3/2, 3/2 state;

$m_1 = 0.96$;

$e_2 = 0.16$.

This formula contains nucleon recoil corrections which do not appear in Reference 65. See Figs. 24, 28, and 30 - 34 for the comparison of the theory with experimental results.

The π^+ angular distributions from hydrogen are usually analyzed in the form $(d\sigma/d\Omega)_{c.m.} = A + B \cos\theta + C \sin^2\theta$. These coefficients can then be related to the π-meson-nucleon scattering phase shifts by use of a phenomenological approach. The present data have not been analyzed in this form, since only two angles were obtained. This type of analysis has been applied by other workers to their data. Some of these data are shown in Figs. 30 - 34. An analysis of this type is shown in Fig. 30 for old Berkeley data[16, 19] for 275-Mev photon. Points from this experiment have been added.

The deuterium-hydrogen ratios have been compared to a phenomenological treatment by Chew and Lewis.[64] Their work is equivalent to that done by Lax and Feshbach,[66] and Saito, Watanabe, and Yamaguchi.[67] The treatment used here is the Method 2 described by White, Jakobson, and Schultz.[16] The basis of the calculation is as follows: Consider the reaction $\gamma + d \longrightarrow 2n + \pi^+$. The deuteron is initially in the ^3S state (96%); therefore, if the proton does not flip its spin relative to the neutron in the production of a meson, then the resulting two-neutron system

can be only in a ^1S, ^3P. . . state. Other states are excluded by the Pauli exclusion principle. This effect reduces the available phase space relative to that for production of a meson on a free neutron or proton. This reduction in phase space in turn reduces the corresponding cross sections. Furthermore, the binding energy of the deuteron also reduces the available phase space, with like reductions in cross sections. Chew and Lewis use these principles to calculate cross sections for the all-spin-flip and the no-spin-flip cases. The calculation uses the Hulthén wave function for the deuteron with $\beta = 6\alpha$ and plane waves for the neutrons in the final state. The results of these calculations in the form of deuterium-hydrogen ratios for π^+-mesons are shown in Fig. 27 and 29 along with experimental points. The $\gamma^2 = 0$ curve is for all-spin interaction, and the $\gamma^2 = 1$ curve is for no-spin interaction. The curves turn upward at high energy because the hydrogen cross sections go to zero at the bremsstrahlung cutoff while there is still a small contribution from deuterium.

Gell-Mann and Watson[68] give $\pi^-/\pi^+ = (1 - \frac{\mu}{M})^2 = 1.32$ (where μ and M are the masses of the π-meson and nucleon respectively) for the ratio of the differential cross sections for π^-- and π^+-mesons from deuterium at low energy. This formula is derived from spin and isotopic spin arguments. This theoretical value agrees with the three experimental values given by this experiment within the experimental error. These values are also compatible with the values of Sands at 140°.[29]

The carbon-hydrogen, helium-hydrogen, and deuterium-hydrogen ratios shown in Fig. 23 indicate that the unbound proton in hydrogen is more effective in producing π^+-mesons than the bound proton in the other three materials. The tightly bound protons in helium and carbon are less effective than the weakly bound proton of deuterium. Possibly, this effect is due to the recoil neutron's having less phase space available in the higher-Z elements because low-energy neutron states are already occupied.

ACKNOWLEDGMENTS

I wish to express my appreciation to Professor Edwin M. McMillan for his guidance and support of my graduate research work. It would be difficult to adequately thank my co-workers, Dr. R. Stephen White and Dr. Mark J. Jakobson, for their aid in every phase of the experiment.

I should also like to thank Mr. Robert C. Mathewson and Mr. Roscoe A. Byrns for their aid in modifying the gas and the liquid targets to meet the necessary requirements and for assisting in keeping the targets in operation. I am also indebted to Mr. Fred Vogelsberg for setting up the pulse-height analyzer, to Mrs. Arthur L. Lloyd and Mrs. Leon K. Parris, Jr. for scanning the emulsions, and to the members of the synchrotron crew for providing the photon beam and assisting whenever possible.

REFERENCES

Charged π-photomeson experiments from various targets:

1. E. M. McMillan and J. M. Peterson, Science 109, 438 (1949).
2. McMillan, Peterson, and White, Science 110, 579 (1949).
3. R. F. Mozley, Phys. Rev. 80, 493 (1950).
4. Peterson, Gilbert, and White, Phys. Rev. 81, 1003 (1951).
5. Camac, Corson, Littauer, Shapiro, Silverman, Wilson, and Woodward, Phys. Rev. 82, 745 (1951).
6. H. A. Medicus, Phys. Rev. 83, 662 (1951).
7. Littauer and Walker, Phys. Rev. 86, 838 (1952).
8. W. F. Dudziak, Phys. Rev. 90, 342 (1953).
9. Jakobson, Schulz, and White, Phys. Rev. 91, 695 (1953).
10. Bandtel, Frank, and Madey, Phys. Rev. 91, 487 (1953).
11. Voss, Palfrey, and Haxby, Phys. Rev. 93, 918 (1954).
12. D. Luckey, Phys. Rev. 97, 469 (1955).

Charged π-photomeson experiments from hydrogen and deuterium:

13. J. Steinberger, and A. S. Bishop, Phys. Rev. 86, 174 (1952).
14. Feld, Frisch, Lebow, Osborn, and Clark, Phys. Rev. 85, 680 (1952).
15. Keck and Littauer, Phys. Rev. 88, 139 (1952).
16. White, Jakobson, and Schulz, Phys. Rev. 88, 836 (1952).
17. Littauer, Perry, and Woodward, Phys. Rev. 90, 342 (1953).
18. Goldschmidt-Clermont, Osborne, and Winston, Phys. Rev. 91, 468 (1953).
19. Jarmie, Repp, and White, Phys. Rev. 91, 1023 (1953).
20. J. E. Carothers, Phys. Rev. 92, 538 (1953).
21. Tollestrup, Keck, and Worlock, Phys. Rev. 92, 1090 (1953), and prepublication report.
22. Walker, Teasdale, and Peterson, Phys. Rev. 92, 1090 (1953), and prepublication report.
23. Janes and Kraushaar, Phys. Rev. 93, 900 (1954).
24. Bernadini and Goldwasser, Phys. Rev. 94, 729 (1954).
25. W. F. Dudziak, Phys. Rev. 94, 756 (1954).

26. Jenkins, Luckey, Palfrey, and Wilson, Phys. Rev. 95, 179 (1954).
27. Robinson and Leiss, Phys. Rev. 95, 638 (1954), and unpublished report.
28. Osborne, Goldschmidt, and Parker, Phys. Rev. 95, 637 (1954).
29. Sands, Teasdale, and Walker, Phys. Rev. 95, 592 (1954).
30. Peterson and Henry, Phys. Rev. 96, 850 (1954).

Neutral π-photomeson experiments:

31. Silverm and Stearns, Phys. Rev. 83, 853 (1951).
32. Panofsky, Steinberger, and Steller, Phys. Rev. 86, 180 (1952).
33. Cocconi and Silverman, Phys. Rev. 88, 1230 (1952).
34. Oakley, Walker, Teasdale, and Vette, Phys. Rev. 93, 949 (1954).
35. Davis and Corson, Phys. Rev. 94, 746 (1954).
36. Goldwasser, Koester, and Mills, Phys. Rev. 95, 1692 (1954).
37. Goldschmidt-Clermont, Osborne, and Scott, Phys. Rev. 97, 188 (1955).

Miscellaneous References:

38. Powell, Hartsough, and Hill, Phys. Rev. 81, 213 (1951).
39. Anderson, Kenney, and McDonald, private communication.
40. H. R. Bowman and R. E. Thomas, Multichannel Pulse-Height Analyzer, University of California Radiation Laboratory Report No. UCRL-2164, April 1953.
41. R. R. Wilson, private communication to A. C. Helmholz.
42. Blocker, Kenney, and Panofsky, Phys. Rev. 79, 419 (1950).
43. H. A. Morewitz and M. H. Shamos, Phys. Rev. 92, 137 (1953).
44. Jakobson, Schulz, and Steinberger, Phys. Rev. 81, 894 (1951).
45. D. H. Stork, Total Positive Pion Cross Sections in Complex Nuclei (Thesis), University of California Radiation Laboratory Report No. UCRL-2288, July 1953.
46. Fowler, Fowler, Shutt, Thorndike, and Whittemore, Phys. Rev. 91, 135 (1953).
47. C. E. Angell, and J. P. Perry, Phys. Rev. 92, 835 (1953).
48. Orear, Lord, and Weaver, Phys. Rev. 93, 575 (1954).
49. Bodansky, Sachs, and Steinberger, Phys. Rev. 93, 1367 (1954).

50. M. J. Jakobson, The Production of Photomesons from Helium (Thesis), University of California Radiation Laboratory Report No. UCRL-1317, May 1951.

51. A. G. Schulz, Jr., The Excitation Function for π^+-Mesons Produced in p-p Collisions at 0° to the Beam (Thesis), University of California Radiation Laboratory Report No. UCRL-1756, May 1952.

52. J. Merritt, Cross Sections for Production of π^+-Mesons by 335-Mev Protons as a Function of Atomic Number (Thesis), University of California Radiation Laboratory Report No. UCRL-2424, November 1953.

53. L. Eyges, Phys. Rev. 74, 1535 (1948).

54. L. L Foldy, Phys. Rev. 75, 311 (1949).

55. Aron, Hoffman, and Williams, AECU-663.

56. F. M. Smith, Meson-Mass Measurements.II on the Measurement of the Masses of Charged Pions, University of California Radiation Laboratory Report No. UCRL-2371, February 1954.

57. Johnston, Bezman, Rubin, Swanson, Corak, and Rifkin, AEC Report MDDC-850.

58. N. Jarmie, The Productions of Mesons by Photons at 0° (Thesis, revised), University of California Radiation Laboratory Report No. UCRL-2159, March 1953.

59. E. C. Kerr, AECD-3211.

60. L. Jones, Excitation Function for Photoneutron Production from 80 to 320 Mev (Thesis), University of California Radiation Laboratory Report No. UCRL-1916, August 1952.

61. J. H. Malmberg, and L. J. Koester, Jr., University of Illinois, Physics Department Report.

62. G. F. Chew, Private communication.

63. Adelman and Jones, Science 111, 226 (1950).

64. Chew and Lewis, unpublished report.

65. G. F. Chew, Phys. Rev. 95, 1669 (1954).

66. Lax and Feshbach, Phys. Rev. 88, 509 (1952).

67. Saito, Watanabe and Yamaguchi, Prog. Theor. Phys. 7, 103 (1952).

68. Gell-Mann and Watson, Ann. Rev. of Nuclear Science 4, 219 (1954).